UNIVERSIDADE DE LISBOA
FACULDADE DE CIÊNCIAS
DEPARTAMENTO DE BIOLOGIA ANIMAL

Exploring the role of the BMP-signaling in the evolution of vertebrate appendages

Francisco Maria Granchinho Bicho Tavares Cadete

Mestrado em Biologia Evolutiva e do Desenvolvimento

Dissertação orientada por:
Dr. Renata Freitas
Dr. José Élio Sucena

2021

Acknowledgements

Almost every day over the last year, I have learnt something new. This has made me develop both personally and professionally, and it would not have been possible without the help and support of many people.

First, I want to thank Dr. José Élio Sucena for accepting my application to the course, which permitted me to embark on this journey, and for all the help provided during the process.

To Dr.Renata Freitas, for welcoming me into the project and guiding me through with so much patience and motivation. I am grateful for all the opportunities, tools, and knowledge that you provided me, allowing me to grow as a scientist and as a person. I would also want to thank all the members of the CGD group. To Simone Bessa, for teaching me so many techniques and the patience that is required. To Miguel Francisco for being my partner in crime, together we faced many challenges, but we managed to complete every quest. Joana Castro for always being cheerful, for the encouraging words, and for being there in the final moments of this adventure.

To my family, I am forever grateful for being there for me and helping me with every need. Lastly, I want to thank all my friends, the old ones back in my hometown and the new ones made in Porto.

Abstract

Vertebrate appendages have undergone several morphological changes that allowed them to explore new environments. One of these changes was the transition from fish fins to tetrapod limbs. Genes in the 5' end of the HOXD cluster are known to regulate limb skeletal formation, in particular *Hoxd13,* which is involved in the formation of the autopod, the most distal structure of the tetrapod limbs. Overexpression of this gene during zebrafish fin development causes endochondral expansion and a concomitant reduction of the finfold, mimicking the major events thought to have happened during fin-to-limb transition. *Bmp2* is a downstream target of the *Hoxd13* encoded transcription factor, and its overexpression also leads to a similar reduction of the finfold. Here we explored how this *hoxd13-bmp2* mechanism mediate finfold size. To this purpose, here we characterized the expression of *BMP-signaling* related genes in three zebrafish lines with distinct finfold size: 1) wild type; 2) *hsp70:hoxd13a* transgenics with shorter finfolds; 3) leo^{t1}/lof^{dt2} mutants with longer finfolds. The results suggest that the BMP signaling is enhanced in transgenics with shorter finfolds and inhibited in mutants with longer finfolds, with genes in this network exhibiting distinct heterochronic dynamics. Our data lead to a more profound understanding of the molecular changes involved in the definition of the finfold size, a structure that was progressively eliminated during the fin-to-limb transition in vertebrates.

Key words: zebrafish; development; finfold; *hoxd13a*; *bmp2b*.

Resumo

A colonização de ambientes terrestres pelos animais vertebrados foi potenciada por mudanças morfológicas que lhes permitiram sobreviver em novos nichos ecológicos. Uma destas mudanças ocorreu nos seus apêndices locomotores, havendo uma conversão das barbatanas em membros com a origem dos tetrápodes, caracterizados por terem uma nova extremidade distal, o autopódio.

Dados fósseis sugerem que a transição entre as barbatanas dos peixes e membros dos tetrápodes envolveu uma expansão sequencial do endosqueleto e uma redução concomitante do dermoesqueleto distal, adaptado para a deslocação em ambiente aquático. Do ponto de vista do desenvolvimento embrionário, os mecanismos iniciais de formação das barbatanas e dos membros são idênticos. Ambos começam com a formação de um botão originado a partir da placa lateral da mesoderme (LPM), seguida pela indução da crista ectodérmica apical (AER). Esta estrutura produz fatores de crescimento de fibroblastos (fgfs) que estimulam o crescimento ao longo do eixo proximal-distal (PD). Simultaneamente, as células do mesênquima posterior formam a zona de atividade de polarização (ZPA), produzindo a proteína Sonic Hedgehog (Shh), uma proteína que se difunde pelo tecido, instigando uma assimetria típica ao longo do eixo ântero-posterior (AP).

Deste ponto em diante, o desenvolvimento diverge entre as barbatanas de peixes e os membros de tetrápodes. Durante o desenvolvimento da barbatana, a AER é transitória e é convertida na prega ectodérmica distal (*finfold*) que corresponde à região onde os típicos raios das barbatanas de peixe se diferenciam.

Em contraste, nos tetrápodes, a AER falha em alongar-se e é mantida durante todo o desenvolvimento do membro até à formação do autopódio. Tendo isto em consideração, foi colocada a hipótese de que durante a transição "barbatana-membro", houve uma mudança heterocrônica na transição de AER para *finfold* que ocorre mais cedo durante o desenvolvimento em actinopterígios, mais tarde em sarcopterígios e está ausente na linhagem dos tetrápodes. Esta mudança heterecrônica levou à regressão progressiva da *finfold* em detrimento da manutenção da AER ao longo da evolução.

Genes da extremidade 5' do cluster HOXD são conhecidos por regularem a condrogénese nos membros dos tetrápodes, em particular o gene *Hoxd13*, que está envolvido na formação do autopode, a estrutura mais distal destes apêndices. Durante o desenvolvimento, o *Hoxd13* é expresso em duas fases distintas. A primeira fase é conservada durante o desenvolvimento das barbatanas de peixes e dos membros de tetrápodes, sendo a sua expressão restrita à margem posterior do membro em desenvolvimento. A segunda fase de expressão expande-se distalmente ao longo do eixo AP, acabando por ocupar toda a região presuntiva do autopódio, e demonstrando uma separação bem definida da primeira fase, quer temporal quer regional. Durante desenvolvimento da barbatana dos peixes, no entanto, este gene tem uma segunda fase de expressão distalmente mas não se expande completamente ao longo do eixo AP.

Considerando os dados anteriores, foi hipotetizado que as mudanças de expressão de *hoxd13* terão sido um dos mecanismos por detrás da transição de barabatana para membro de tetrápode. Para testar esta hipótese, Freitas e colegas (2012) imitou esta segunda fase de expressão de membros de tetrápodes durante o desenvolvimento da barbatana e peixe-zebra, gerando transgênicos onde é possível induzir a sobrepressão de *hoxd13a* logo antes da segunda fase de expressão. A sobrepressão deste gene durante o desenvolvimento da barbatana do peixe-zebra causa expansão endocondral e uma redução concomitante

da *finfold*, simulando os principais eventos que se acredita terem acontecido durante a transição de barbatana para o membro.

Num estudo recente do laboratório de acolhimento (Castro et al, 2021), foi investigado o impacto da sobrepressão de *hoxd13a* em alvos putativos a jusante deste gene durante o desenvolvimento da barbatana de peixe-zebra. Um dos resultados mais notórios consequentes desta sobrexpresssão foi a expressão ectópica de várias proteínas morfogénicas ósseas (BMP) na barbatana com *finfolds* truncados. Em tetrápodes, já foi observado que *bmp2* é um alvo direto do factor de transcrição *Hoxd13*. De modo a entender melhor o papel do *bmp2* na transição de barbatana para membro, estes autores geraram peixes-zebra transgênicos, que permitem a sobrepressão de *bmp2b* antes do início da segunda fase de expressão dos genes 5'HoxD. Estes transgênicos apresentaram um fenótipo semelhante ao encontrado nos peixes transgênicos com sobrepressão de *hoxd13a*, apresentando uma redução da *finfold*. Curiosamente, quando *Bmp2* é inibido em ratos durante o desenvolvimento dos membros, existe uma elongação da AER, revelando semelhanças com a transição de AER para finfold observada no desenvolvimento de barbatanas. Com isto em mente, a hipótese surgiu de que a modulação da transcrição do *hoxd13* pode ter regulado o tamanho das *finfolds* durante a evolução dos vertebrados induzindo a expressão de *bmp2* e incrementando o processo apoptótico nesta estrutura. Assim, é possível que a sinalização intracelular atribuída às proteínas BMP, e que tem revelado ser crucial a tantos processos biológicos, tenha sido a fonte de mudança no desenvolvimento dos apêndices locomotores durante a evolução.

Neste projeto, exploramos como o *Hoxd13* e seu alvo a jusante, *Bmp2*, regula o tamanho das *finfolds* durante o desenvolvimento da barbatana de peixe-zebra. Para este fim os seguintes objetivos foram traçados para este projeto:

1) Caracterizar como a sinalização de BMP varia entre três linhas de peixe-zebra com tamanhos de *finfold* distintos: a linha tipo selvagem (*wtAB*), a linha mutante com *finfolds* longas (leo^{d1}/lof^{dt2}) e a linha transgénica com *finfolds* curtas que sobrexpressa *hoxd13a* (*hoxd13 +++*).

2) Comparar a dinâmica de expressão de *bmp2* e outros genes envolvidos na sinalização de BMP *(smad1*, *smoc1*, *smoc2*, *nogg3*, *grem1a* e *msx2b*) entre estas distintas linhas de peixe-zebra ao longo de vários estádios de desenvolvimento (desde as 24 até às 120 horas após fertilização).

Os resultados da caracterização da sinalização de BMP através de análise de imunofluorescência sugerem que esta é aumentada em transgênicos com *finfolds* mais curtas e diminuída em mutantes com *finfolds* mais longas. Olhando para a expressão de *bmp2b*, os mutantes leo^{d1}/lof^{dt2} demonstram menos expressão deste gene do que na linha *wtAB* e tendo picos de expressão ligeiramente deslocados para estádios mais tardios em relação à linha tipo selvagem. Em relação aos transgênicos *hoxd13 +++*, a expressão de *bmp2b* demonstra um pico de expressão logo após a sobrexpressão de *hoxd13a*, seguindo por uma diminuição até estádios mais tardios onde a expressão volta a aumentar.

Curiosamente, este não foi o único gene encontrado sobrexpresso em resposta à sobrexpressão de *hoxd13a*. Genes como *grem1a*, *msx2b*, *smoc1* e *smoc2* mostraram também uma regulação positiva após o início da sobrexpressão do gene *Hox*. Como nenhum destes genes foi identificado anteriormente como alvos diretos a jusante de *Hoxd13*, a influência deste factor de transcrição sobre estes genes poderá ser indireta, como é o caso do *msx2b*, um gene apoptótico, que foi identificado como sendo controlado diretamente por sinalização BMP em tetrápodes.

Neste estudo, foi observado também que o perfil de expressão do gene *msx2b* segue um perfil muito semelhante ao observado para *bmp2b*, em todas as três linhas analisadas. Estes resultados levam a crer que a sinalização de BMP leva à ativação de mecanismos apoptóticos que poderão influenciar o tamanho da *finfold* através de morte celular programada, à semelhança do que se sucede aquando da perda da membrana interdigital durante a formação dos dígitos dos autopódios em tetrápodes.

Tendo estes dados em consideração, propomos que a redução do tamanho da *finfold* durante a transição de barbatana para membro poderá ter sido mediada pelo aumento da expressão de *Hoxd13*, promovendo níveis mais altos de sinalização de BMP, que então regulam positivamente a expressão de genes apoptóticos distalmente e levam a uma redução do tamanho das finfolds ao longo da evolução.

Palavras-chave: peixe-zebra; desenvolvimento; *finfold*; *hoxd13a*; *bmp2b*.

Table of contents:

List of tables

List of Figures

List of abbreviations

AER	Apical Ectodermal Ridge
AF	Apical Ectodermal Finfold
And	Actinodin
AP	Anterior-posterior
BMP	Bone Morphogenetic Protein
BSA	Bovine Serum Albumin
cDNA	Complementary DNA
CN	Negative Control
co-SMAD	Co-mediator SMAD
CT	Threshold Cycle
cyp26b1	Cytochrome P450 Family 26 Subfamily B Member 1
DABCO	1,4-diazabicyclo[2.2.2]octane
DMSO	Dimethyl sulfoxide
DNA	Deoxyribonucleic acid
dNTP	Nucleoside triphosphate
Ed	Endoskeleton
EGFP	Enhanced green fluorescent protein
Fgf	Fibroblast growth factor
FW	Forward
g	Gravitational force
Grem	Gremlin
GS	Goat Serum
H2O	Water
H_2O D|R	DNAse/RNAse treated H_2O
hpf	Hours post fertilization
HSPG	Heparan sulfate proteoglycans
i3S	Instituto de Investigação e Inovação em Saúde
IBMC	Instituto de Biologia Molecular e Celular
Id1	Inhibitor Of DNA Binding 1
IMF	Immunofluorescence
I-SMAD	Inhibitory SMAD
MeOH	Methanol
$MgCl_2$	Magnesium chloride
Msx	Muscle segment homeobox genes
Nogg3	Noggin 3
o/n	Overnight
PBS	Phosphate-buffered saline
PBT	PBS 1x with 0.1% Tween-20
PCR	Polimerase Chain Reaction
PD	Proximal-distal

pea3	Olyomavirus enhancer activator 3
PFA	Paraformaldehyde
p-SMAD1/5/9	Phosphorylated SMAD1/5/9
RA	Retinoic acid
RNA	Ribonucleic acid
rpm	Revolution per minute
R-SMAD	Receptor-regulated SMAD
RT	Room Temperature
RT-qPCR	Real Time - Quantitative Polimerase Chain Reaction
RV	Reverse
SD	Standard deviation
Shh	Sonic Hedgehog
Smoc	SPARC Related Modular Calcium Binding
TAE	Tris-Acetate-EDTA
Tbx	T-box
Tris-HCL	Tris hydrochloride
wtAB	Wild-Type AB
ZPA	Zone of Polarizing Activity

1-INTRODUCTION

1.1-Origin of locomotory appendages

Throughout evolution animals have evolved a variety of different appendages adapted for sensing, feeding, locomotion, and other functionalities. These appendages generally are formed by multiple tissues (epidermis, muscle, cartilage, bone and nerve) that together form highly complex structures [1]. A particular type of appendages that are quite diverse among vertebrates are the locomotory appendages (Fig.1.1).

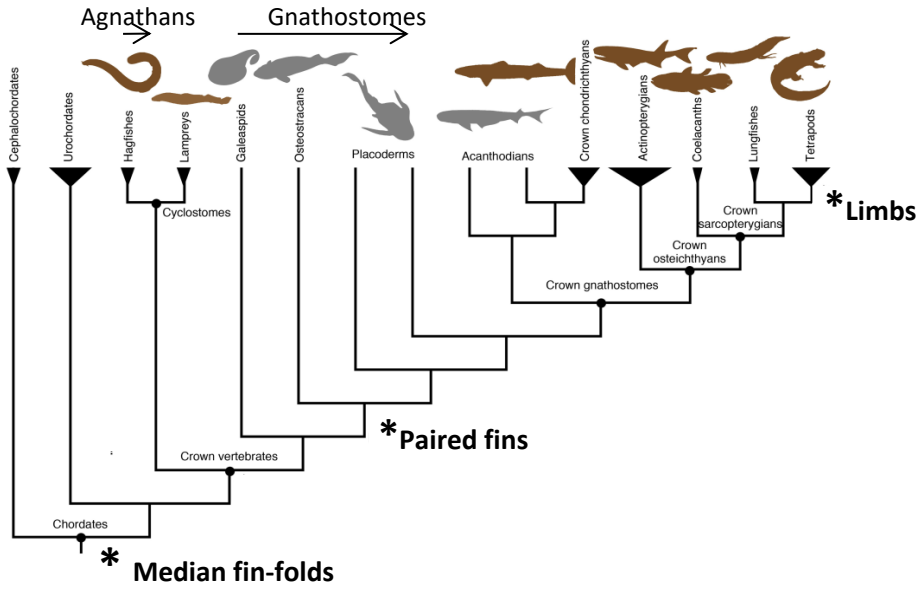

Figure 1.1: Evolution of locomotory appendages. A simplified cladogram of major vertebrate lineages and their outgroups. Asterisks mark novel morphological characters in locomotory appendages. Adapted from [2].

The most ancient locomotory appendages within chordates, arouse during the Pre-Cambrian, and consisted in continuous finfolds that ran through the dorsal and ventral midlines of the body, and that are still detectable in extant cephalochordates, such as the amphioxus [3]. Then, individual median or unpaired fins emerged from these original finfolds, which became detectable only in embryonic stages of fish. Throughout evolution, these individualized unpaired appendages have persisted and can be seen in extant agnathans (e.g. lampreys) and gnathostomes (e.g. sharks). According with their localization, they are designated as dorsal, anal, and caudal fins (Fig. 1.2).

Paired appendages first appeared in agnathans during the Cambrian Era, growing in a lateral-ventral manner through the surface of the body [4]. Two classical theories have been proposed to explain the origin of paired appendages (Fig. 1.2).

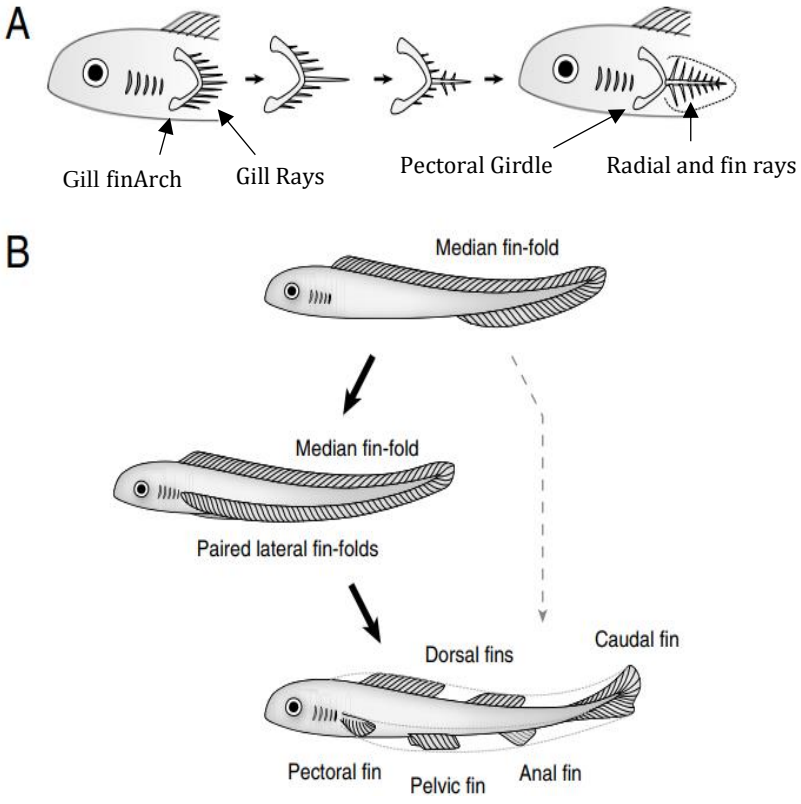

Figure 1.2: Origin of paired fins theories. A) The Gill Arch Theory: paired pectoral finds derived from modified gill arches and rays. B) The Fin-fold Theory: paired fins originated from a continuous lateral fin-fold that became discontinuous giving rise to pectoral and pelvic fins. Adapted from [5].

The Fin-fold or Lateral Fin-fold theory proposed by Thacher, Mivart and Balfour [6-8] that states that paired appendages evolved from a longitudinal bilateral continuous finfolds that extended from the median finfolds (Fig.1.2). This theory was supported by anatomical and developmental similarities between paired fins and median fins in fishes [9] and by the fossil record of Anaspids that present indeed these type of finfolds [10].

Alternatively, the Gill Arch Theory, proposed by Gegenbaur [11] states that paired appendages arose from modified gill arches, where a gill arch gave rise to the pectoral girdle and the gill rays to the fin itself (Fig.1.2). This process gave rise to the pectoral fins and later the supporters of this theory proposed that the pelvic fins arose by co-option of the pectoral developmental program [2]. Although these theories were postulated in the XIX century, no scientific consensus was achieved regarding which theory is correct. However, most researchers are more receptive to the fin-fold theory or to modern views of this

theory that suggest that pectoral fins emerged due to the establishment of a field of competence in the lateral plate mesoderm inherited from the tissue that forms the unpaired fins, the paraxial mesoderm [9].

1.2-The evolution of vertebrate appendages (fin-to-limb transition)

All tetrapod limbs are derived from ancestral fins from Devonian fish and share with them key elements of the bone structure (endoskeleton) [12, 13]. Interestingly, once the main structure of the limb was established in stem groups of tetrapods, it became highly conserved throughout the distinct tetrapod groups, which represent one of the greatest examples of homology in nature, recognized since the XIX century by Darwin [14]. It is thought that the transition from fins to limbs offered an outstanding advantage for the invasion of terrestrial environments, an evolutionary process that was crucial for the origin of the extant vertebrates [4]. This morphological transition from fish fins to tetrapod limbs implicated a progressive reduction of the distal dermoskeletal structures and concomitant increment of the endoskeleton ones, culminating with the origin of a novel multifinger extremity, designated as the autopod [15, 16] (Fig. 1.3 A and C).

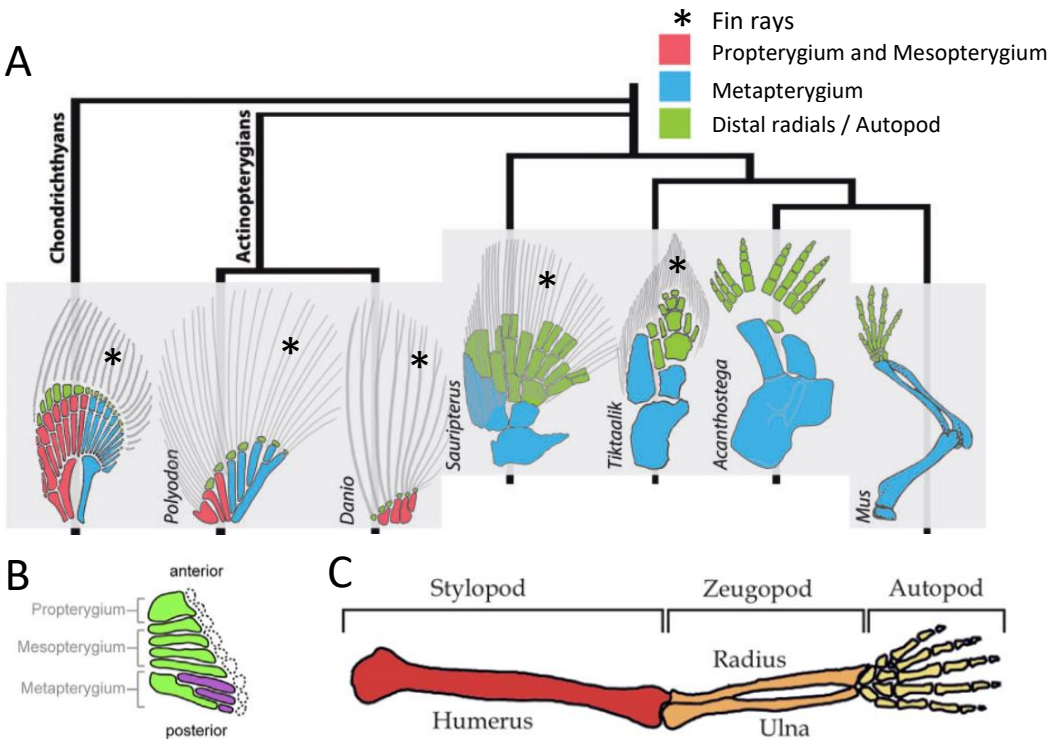

Figure 1.3: Representative schemes of endoskeleton and dermoskeleton structures in vertebrates. A) Locomotory appendages in Vertebrates. Throughout the fin-to-limb evolution there was a continuous elongation of the endoskeleton structures (blue and green) and a concomitant regression of the dermoskeleton structures (grey). Adapted from [1]. B) Bony fish ancestor endoskeleton structures. Adapted from [17]. C) Schematic representation of the skeletal elements of tetrapod limbs. Adapted from [18].

It is hypothesized that the fins of bony fish ancestors, had an endoskeleton composed of a series of radials (homologous to the propterygium, mesopterygium and metapterygium of extant species), placed along the anterior-posterior (AP) axis, with small nodular radials distally, followed by the dermoskeleteon fin rays (Fig. 1.3 B) [19]. During evolution, tetrapod limbs lost the propterygium and mesopterygium, with a continuous elongation of the metapterygium radials leading to the tripartite bauplan known today, composed by the proximal stylopod, the zeugopod and the autopod (Fig. 1.3 C). One extinct species that represents well this elongation of the endoskeleton and regression of the fin rays, is the *Tiktaalik roseae*, one of the first species to conquer the land [20]. This sarcopterygian species retains a reduced dermoskeleton and possess long endoskeleton bones containing several joints.

1.3-Tetrapod limb and fish fin development

From a developmental point of view, the mechanisms responsible for the initiation of fins and limbs are well conserved. The involvement of T-box genes *4* and *5* in this process is a good example of that. Phylogenetic analyses show that these genes are functional paralogs of an ancestral *Tbx4/5* present in jawless vertebrates [21]. *Tbx4* plays major roles in pelvic fin and hindlimb initiation while *Tbx5* expression is a major triggers of pectoral fin and forelimb initiation [22]. Both encode transcription factors that then activate a cascade of molecular events that culminates with the induction of an epithelial-to-mesenchymal transition followed by cell migration from the lateral plate mesoderm to the presumptive bud region [23, 24]. *Tbx5*, together with *Meis1* and *Meis2*, which belong to the TALE homeodomain transcription factor family, induces the expression of fibroblast growth factor 10 (*Fgf10*) in the fin/limb-bud mesenchyme (Fig. 1.4) [25]. *Fgf10* initiates the formation of the apical ectodermal ridge (AER), that corresponds to a thicken layer of the ectoderm in the distal portion of the bud, by inducing the expression of *Wnt* and *Fgf8* genes (Fig. 1.4). The AER is the first signaling domain in the growing fin/limb bud and *Fgf8* maintains *Fgf10* expression in the underlying mesenchyme, creating a *fgf10-fgf8* positive feedback loop [26]. Thus, the AER establishes the distal domain of the fin/limb bud and promotes cell proliferation and growth throughout the proximal-distal (PD) axis. Simultaneously, cells from the posterior mesenchyme, designated as zone of polarizing activity (ZPA), produce sonic hedgehog (Shh), a protein that diffuses throughout the rest of the fin/limb bud, instigating the typical asymmetry along the anterior-posterior (AP) axis. A positive feedback loop is then established between the AER and the ZPA, by the *SHH-GREM1-FGF* regulatory loop, this loop is essential for both AER and ZPA maintenance [27].

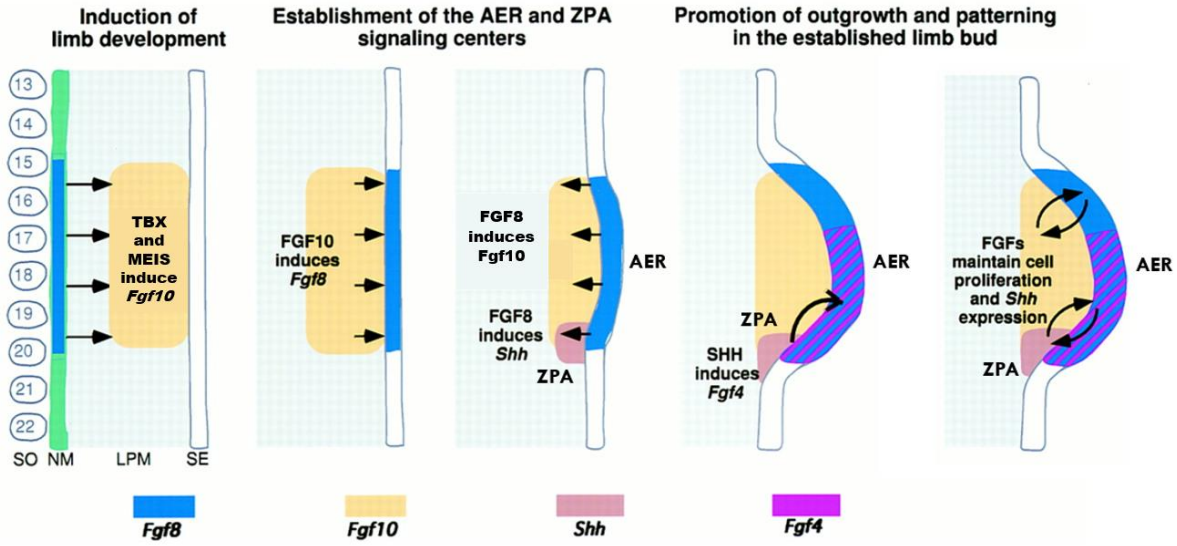

Figure 1.4: Representative scheme of limb/fin bud initiation. During early limb/fin development a positive feedback loop between Shh from the ZPA and Fgf signalling produced in the AER, leading to the maintenance of growth and polarity of endoskeleton structures Adapted from [28].

From this point on the development diverges between fish fins and tetrapod limbs. During fin development the AER is transient and is converted into an apical ectodermal finfold (AF) [29]. In contrast, in tetrapods, the AER fails to elongate and is maintained during the differentiation of the limb structures, the stylopod, zeugopod and autopod [30]. This led Thorogood to propose the "clock model" to explain the fin-to-limb transition, which states that the transition from an AER to AF hinders mesenchyme expansion in fish, and thus inhibits distal endoskeletal formation [31]. In recent years, some developmental studies have given strength to Thorogood model [32].

For example, during zebrafish fin development somite cells migrate to the AER, immediately before the AER-AF transition, this cells are actinotrichia-forming cells, which express *actinodin1* and *actinodin2 (and1* ; *and2)* in the finfold [33].Ablation of this migrating cells disrupts AF induction and leads to an expansion of the underlying mesenchyme [34]. The same phenotype can be observed when *and1* and *and2* are knocked down [33]**.**

In Australian lungfish (*Neoceratodus forsteri*), a sarcopterygian fish, the ZPA disappears around the same time that the AER is converted into a AF [35]. The same seems to occur also during the development of fins in actinopterygian fish, reported in zebrafish (*Danio rerio).* In this case, when finfold development is perturbed, the ZPA is extended [33], proven by maintenance of *Sonic hedgehog* expression (*Shh*) for longer [36]. This suggests that the formation of the finfold may lead to the termination of the ZPA, acting as a barrier between epithelial FGF signalling and mesenchymal ZPA signalling [35].

Together these data suggests that during the fin-to-limb transition there was an heterochronic shift in the AER-to-AF transition which occurs earlier during development in actinopterygians, later in

sarcopterygians and being absent in tetrapods [34, 37]. This heterochronic shift led to progressive regression of the AF in detriment of a maintenance of the AER throughout evolution, promoting an expansion of the distal endoskeleton structures [1, 32].

1.4-*Hox* genes in the fin-to-limb transition

Hox genes are considered one of the major drivers of morphological evolution in the animal kingdom [38]. They belong to the homeobox gene family and encode transcriptional factors essential for animal development that define segmental identity along the AP axis of the body. *Hox* genes are distributed in clusters, being subdivided into 13 groups (Fig. 1.5). Invertebrates only have a single *Hox* cluster, whereas most extant vertebrate lineages have four clusters resultant from two rounds of whole-genome duplications. In teleost, an additional round of whole-genome duplication took place and, therefore, these fishes may present 8 *Hox* clusters instead of 4. However, gene loss events occurred after that in particular species, such as the zebrafish, that seems to have lost an entire *Hox* cluster and several genes within the other clusters (Fig. 1.6) [39].

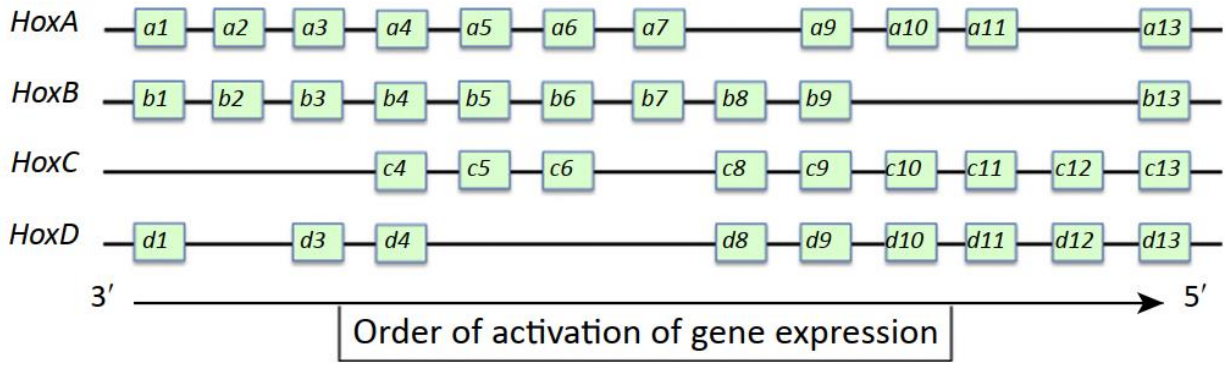

Figure 1.5: *Hox* gene cluster organization in mammals. Adapted from [39].

Each cluster of *Hox* genes is subdivided into 13 groups, based on their position in the cluster (Fig. 1.5), starting with *Hox1* in the 3' end rising to the *Hox13* in the 5' end. Hox gene transcriptional activation follows this 3'-to-5' order which makes *Hox1* the first to be expressed and in more anterior domains during development followed sequentially by the genes located 5' to it, which become expressed sequentially along the AP axis, a phenomenon called spatial and temporal collinearity (Fig. 1.6) [39].

Regarding limb development, *Hox* genes play essential roles, starting by influencing limb and non-limb domains through the AP axis of the embryo, controlling, together with retinoic acid (RA), where the limb initiation will occur [41].

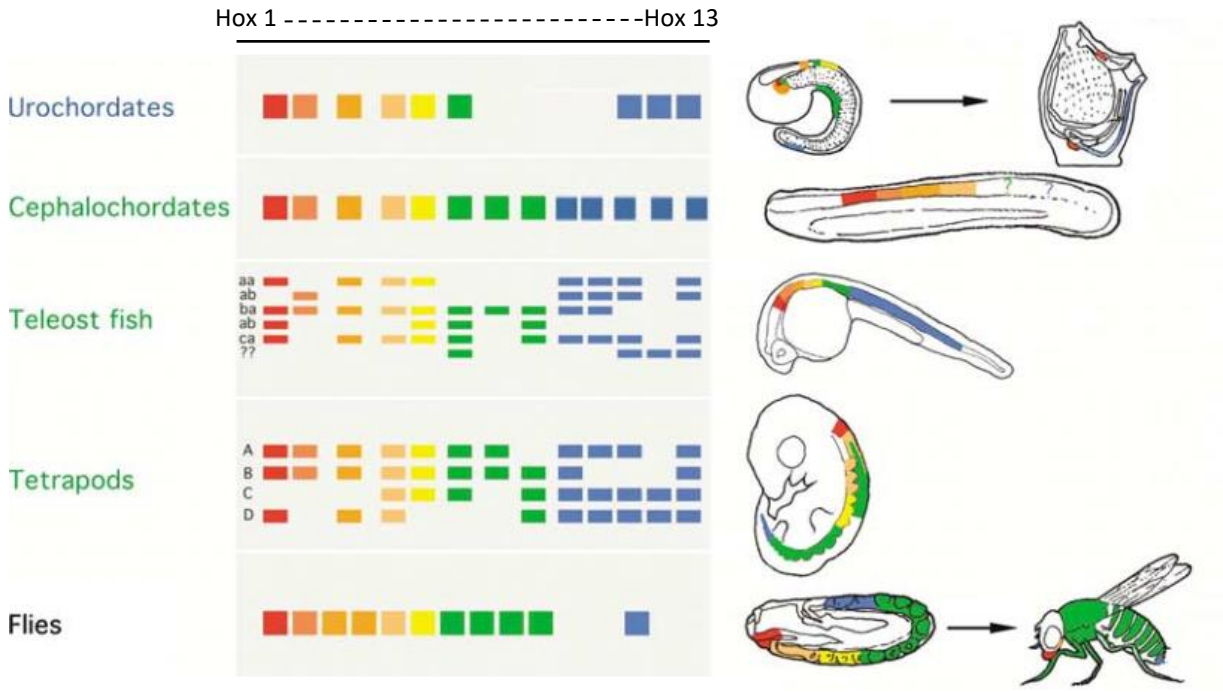

Figure 1.6: Schematic representation of *Hox* gene clusters and expression patterns in different animal models. In the left panel there is a representation of the genomic organization of Hox genes and in the right the expression patterns during development. It is worth mention the effect of spatial collinearity, where further 5' end genes are progressively expressed more posteriorly. Adapted from [40].

Genes located in the 5' of the *HoxA* and *HoxD* cluster have been shown to have major roles in patterning limb development in tetrapods [42], whereas most genes from *HoxB* and *HoxC* were thought to have almost no role in limb development. However some studies have been showing the contrary, for example, *Hoxa5*, *Hoxb5* and *Hoxc5* act has a *Shh* repressor in the forelimb [43].

During limb development *5' HoxD* genes are expressed in two very distinct phases. The first phase regulates the development of proximal endoskeleton elements, where *HoxD9-HoxD12* genes are sequentially expressed forming the so-called "Russian doll" expression domains, and together with *Hoxa11*, *Hoxa13*, and *Meis1* pattern the PD axis until the boundary between the prospective zeugopod and autopod. (Fig. 1.7) [32, 44]. This first phase of expression seems to be conserved in paired fin development in fish (Fig.1.7), but its origin appears to be even before the origin of paired appendages, has this mechanism seems to be present during the formation of the median fins in lampreys and sharks [37]. Thus, this PD patterning mechanism provided by *5' HoxD* gene expression evolved in the formation of median fins and was probably co-opted to the development of paired appendages [37].

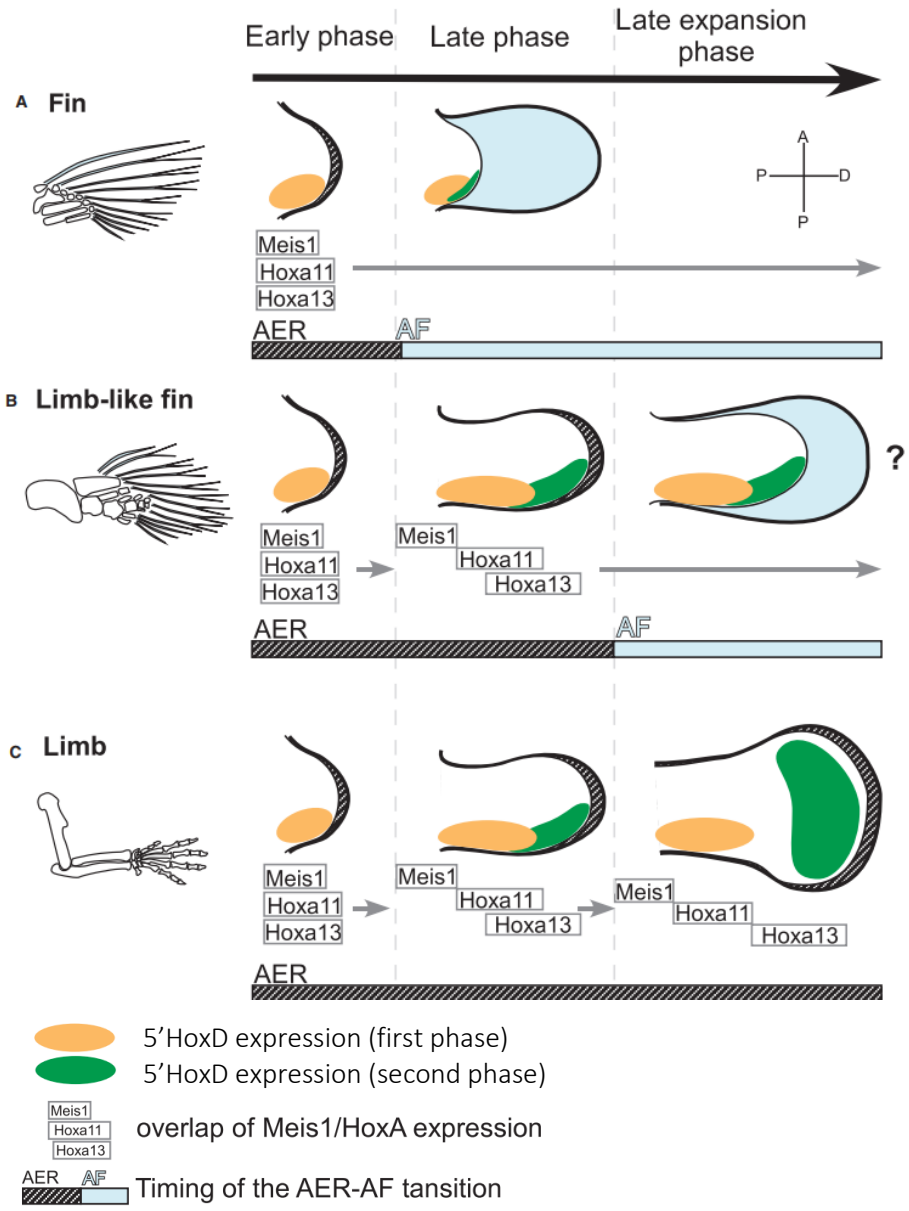

Figure 1.7: Schematic representation of fin and limb development. A – In fin development *5'HoxD* expression is confined in the posterior domain of the fin during the first and second phase of expression (yellow and green respectively) and the AER is rapidly converted into AF. B- Limb-like fin, an intermediate phenotype between fin and limb, the second phase of expression of *5'HoxD* is speculated to be prolonged and to expand more anteriorly, concomitant with a later AER-AF transition, resulting in more pronounced endoskeleton with fin rays. C- Tetrapod limbs do not undertake the AER-AF transition, and the AER is present until autopod formation, contrary to the other examples the second phase of expression totally expands anteriorly occupying the prospective autopod region, this results in very elongated endoskeleton with total absence of dermoskeleton structures. Adapted from [44].

The second phase of expression is essential to the formation of the autopod, the evolutionary novelty that characterizes the tetrapod limb, and is characterized by the expression of *Hoxd11*, *Hoxd12*, and *Hoxd13*.

While in the first phase of expression of these genes are confined to the posterior mesenchyme of the limb, during this second phase it starts to expand anteriorly, with *Hoxd13* occupying all the prospective region of the autopod and showing a spatial and temporal separation from the first phase (Fig. 1.7) [44, 45]. This second phase of expression is also present during fin development, detected in zebrafish and in species representing key phylogenetic positions such as chondrichthyans (*Scyliorhinus*), basal actinopterygians (*Polyodon*), and basal sarcopterygians (*Neoceratodus*) [37, 46-48]. However, this phase of expression does not recapitulate the one present in tetrapods, being these *5' Hoxd* genes confined to the most distal mesenchyme, in sharks for example, or not fully expanding anteriorly, observed in zebrafish (Fig. 1.7) [37, 46-48].

In tetrapods these distinct phases of expression are activated by independent *cis*-regulatory regions located either in the telomeric or centromeric flanks of the *HoxD* cluster, being the second phase deriven by elements in the centromeric region [49, 50]. In fish the presence of this distinct types of *HoxD* transcriptional modulation have been questioned because of the distinct second phase of expression of these genes between tetrapods and zebrafish [51], but recent studies suggested that zebrafish *HoxD* loci has also two topological domains at an epigenomic level [52]. Transgenic approaches have shown that zebrafish regulatory landscapes of the *HoxA* an *HoxD* clusters triggered transcription of these genes proximally instead of distally in mice [52]. Contrarily when mice enhancers were placed into zebrafish, they were able to drive expression of these genes in distal fin mesenchyme [36, 53]. These findings suggest that most regulatory mechanisms used to pattern tetrapod limbs preceded the divergence of fish and tetrapod and that the tetrapod novelty, the autopod, arose through the acquisition of novel regulatory elements [36], leading to the anteriorization and higher expression of *hoxd13*, one of the genes involved in autopod formation.

Taking these into consideration, Freitas and colleagues developed transgenic zebrafish lines that allowed the overexpression of *hoxd13a* during the second phase of expression, mimicked the same event that occurs during tetrapod limb development [36]. In these experiments, these authors detected distal production of chondrogenic tissue and upregulation of autopod markers such as *hoxa13b*, *cyp26b1* and *pea3*. Concomitant to this, there was a reduction of the AF, in which the dermoskeleton develops [36]. This phenotype resembles what is thought to have happen during the fin-to-limb transition. In addition to this, a survey conducted in mice showed that when there is reduction of *Hoxa13* and 5´HoxD genes the digits developed thinner and more packed, resembling the endoskeleton pattern of fish fins [54]. These results suggest that the modulation of *hoxd13* during evolution influenced the fate of distal cells by inducing differentiation into endochondral bone rather than dermoskeleton, reducing the AF in detriment of a maintenance of the AER.

1.5: *Hoxd13/Bmp2* influence in finfold formation.

Hoxd13 expression is required for the patterning of the most distal limb region, and the induction of overexpression in zebrafish fin development leads to a more limb-like development, recapitulating what is hypothesized to have happened during the fin-to-limb transition [36]. Although the modulation of

Hoxd13 expression during evolution is thought to have been crucial for the limb-to-fin transition, the *Hoxd13*-associated molecular mechanisms that promoted this transition are still not well identified.

A recent Chip-to-chip analysis, performed in chick embryos, led to the identification of several *Hoxd13* downstream targets that are relevant for limb patterning and chondrogenesis [55]. One of these identified genes was *Bmp2*. These genes encoded a Bone Morphogenetic Protein (BMP), which is part of the Transforming Growth Factor-b (TGF-b) superfamily of proteins and carry out a diverse array of functions during embryonic and postnatal development, homeostasis, and disease [56]. During early development, the signaling promoted by BMP proteins (BMP-signaling) influences cell growth, differentiation, and apoptosis [57]. The BMPs are signaling molecules that when secreted to the extracellular environment can influence distant cells and create gradients of concentration [58]. Moreover, the BMP signaling can act via a canonical and noncanonical pathway. In the canonical pathway, the signal transduction cascade is initiated by the binding of the BMP ligand to its cognate serine/threonine kinase receptor. Upon this binding with the cell surface receptors, a hetero-tetrameric complex is created, consisting of two dimers of type I and type II BMP receptors. When this happens, type II receptors phosphorylate type I receptors, which will phosphorylate the downstream substrate proteins present in the cytosol, the receptor-regulated SMADs (R-SMADs). The R-SMADs involved in BMP-signaling are SMAD1, SMAD5, and SMAD8 or 9 (SMAD1/5/9), when phosphorylated (p-SMAD1/5/9) they associate with the co-mediator SMAD (co-SAMD) SMAD4 and this complex travels to the nucleus and act as a transcription factor for BMP gene targets (Fig.1.8) [56].

BMP-signal duration and strength can be regulated at many levels: intracellularly by expression levels, inhibitory SMADs (SMAD6 and SMAD7) (Fig.1.8), methylation, and miRNAs, and extracellularly by BMP antagonists [59]. Noggin and Gremlin are secreted antagonists that block BMP signaling preventing BMP ligand to bind to its receptors [60] (Fig.1.8). On the other hand, SMOC1 and SMOC2 act as antagonists and BMP signaling by binding to heparan sulfate proteoglycans (HSPGs) present in the extracellular matrix, which normally interacts with BMP and restricts its diffusion [61].

During the initiation of limb development, BMP activity is high and contributes to the establishment of the AER. Afterward, however, the BMP activity diminish due to the action of antagonists, such as Gremelin 1 (*Grem1*), activated by the SHH signaling from the ZPA. This will allow the *SHH/GREM1/AER-FGF* feedback loop to be established, resulting in upregulation and anterior expansion of the AER, which controls distal growth. BMP activity rises again in later stages, promoting progenitor mesenchymal cells to enter chondrogenesis and, eventually, participating in digit identification and interdigital cell death [56].

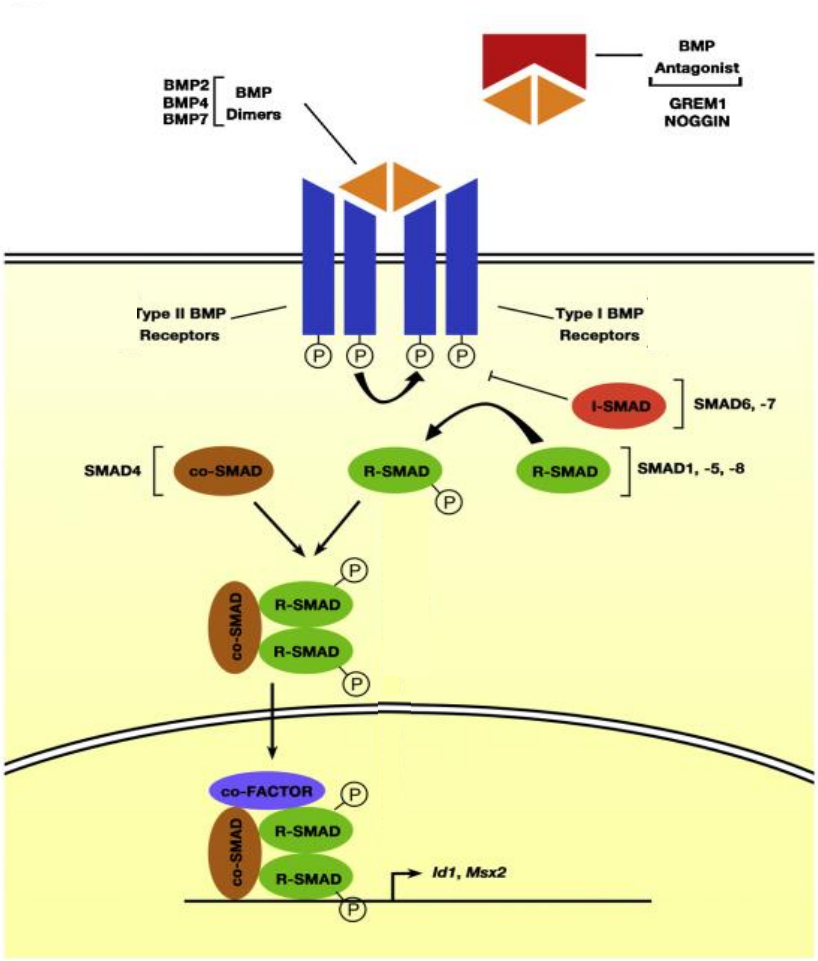

Figure 1.8: BMP-signaling pathway. The scheme represents the canonical pathway of BMP-signaling in limb bud development. BMP ligand dimers BMP2, BMP4, and BMP7 interact with their receptors, inducing the Type II receptor to phosphorylate of Type I receptor which will activate, via phosphorylation, the R-SMADs, SMAD1, -5 and -8/9. The phosphorylated R-SMAD will associate with SMAD4 and this complex will travel to the nucleus and regulate the expression of BMP target genes, such as *Id1* and *Msx2* in limb bud development. Antagonists like GREM1 and NOGGIN bind to BMP ligands preventing them from binding with its receptors in the extracellular matrix, whereas inhibitory SMADs (I-SMADs), like SMAD6 and SMAD7 block BMP-signaling transduction in the cytoplasm. Adapted from [56].

In a recent study from our lab [62], it has been investigated the impact of *hoxd13a* overexpression in putative downstream targets during zebrafish fin development. One of the main results was that *hoxd13a* overexpression leads to the ectopic expression of several BMPs in the shortened finfolds, such as *bmp2b*. To further understand the role of *bmp2b* in the fin-to-limb transition transgenic zebrafish were generated allowing the overexpression of *bmp2b* just before the initiation of the second phase of *hoxd13a* expression [62]. This second phase of expression has been associated in tetrapods to the development of the autopod and the aim was to identify if overexpression of a putative *hoxd13* target may also cause finfold truncation. As predicted, these transgenic fish showed a phenotype resembling the one found in transgenic fish with *hoxd13a* overexpression, presenting a reduced finfold. Interestingly, when *Bmp2* is inhibited in mice during limb development this leads to an elongation of the AER, resembling a finfold. [63]. This led to the hypothesis that, throughout limb-to-fin evolution, finfold loss may have been achieved through modulation of BMPs distally, mediated by *Hoxd13*.

2-AIMS

Hoxd13, a transcription factor known to be required for autopod development in tetrapods, is thought to play a key part in the fin-to-limb transition in vertebrates. This transition involved the continual expansion of the endoskeleton and the simultaneous reduction of distal dermoskeleton components. The shortening of the finfold, the presumptive structure from which the dermoskeleton differentiates, is hypothesized to have been one of the processes involved in the fin-to-limb transition. In this project, we explored how *Hoxd13* and its putative downstream target, *Bmp2*, regulate finfold size. We hypothesize that during the evolutionary transition from fish fins to tetrapod limbs, the modulation of BMP-signaling was altered, causing inhibition of finfold expansion during development. To this end, the following aims were pursued in this research project:

1) Characterize how BMP-signaling varies amongst three zebrafish lines with distinct finfold-sizes: *wild-type* condition *(wtAB)*, the long finfold *leo*^{d1}*/lof*^{dt2} condition, and the short finfold *hoxd13a overexpressing* condition *(hoxd13+++)*.

2) Compare the expression dynamics of *bmp2* and other genes involved in the BMP-signaling between the distinct zebrafish lines (*wtAB, leo*^{d1}*/lof*^{dt2}*, hoxd13+++*).

3-METHODOLOGY

3.1-Zebrafish husbandry, breeding, and manipulation

3.1.1-Reproduction, egg collection

All the experiments followed the European Union Animal Research Guidelines, and the experimental design was approved by the Ethics Committee of IBMC/I3S and DGAV (Portugal). As stated above, three zebrafish lineages were used in this project, *Wild-type AB* (*wtAB*), the Tüpfel-longfin mutant (*leo*^{t1}/*lof*^{dt2}), and the *hsp70:hoxd13a* transgenic lines. Adult fish were kept in the i3S fish facility, in water tanks with the following conditions: 27.5ºC, pH between 6.8 and 7.5, and a photoperiod of 14h-light/10h-dark cycle. Adult fish were used only to generate embryos, which were used in experiments, or to produce breeders.

To obtain embryos for the experiments, incross breeding was performed between fish of the same line, to control genetic variability. Afterward, eggs are collected and placed in E3 solution, a medium that contains methylene blue and avoids fungi proliferation. The embryos were placed developing in incubators at 28.5ºC, a temperature that makes it possible to stage the embryos according to Kimmel *et al* [64] each stage corresponds to 1 hour of development at that temperature. However, in some cases the temperature of the incubator was manipulated to fasten or retard the development depending on our needs, the temperatures were selected following Kimmel *et al* table of development rates [64].

3.1.2-Heat-shock treatment

Heat-shock treatments were conducted in *hsp70:hoxd13a* embryos to induce the overexpression of *hoxd13a*. To this end, we selected the transgenic embryos at 24hpf by searching for green fluorescence signal in the developing hearts, using a stereoscope. This signal was due to the activation of the *cmlc2* promoter associated to the reporter gene *EGFP* present in the construct allowing hoxd13a overexpression [36]. The heat-shock activated another promoter within the construct (*hsp70*) that leads to the ectopic transcription of *hoxd13a*. This procedure consisted in immersing the embryos in water at 38,5ºC for 1 hour and it was first performed at 30hpf. The rationale behind the choice of this particular stage was the fact that the second wave of *5'Hoxd* gene expression, which in tetrapods gives rise to the formation of the autopod, was described to occur in zebrafish at 32hpf. Therefore, by causing the heat-shock two hours before the *5´Hoxd* gene second wave, we could ensure high levels during that wave mimicking the levels of expression during tetrapod limb development. Afterward, to maintain the levels of *hoxd13a* high, this treatment was repeated every 24 hours, starting at 48hpf until the desired developmental stage.

3.1.3-Fixation and dehydration of embryos

Upon reaching the desired developmental stage, embryos destined to immunofluorescence (IMF) protocols, were fixed in 4% PFA (paraformaldehyde) overnight at 4ºC. The day after, they were washed in increasing methanol concentrations. Each passage had the duration of 5 minutes and was done on ice and in the shaking platform, following the order: PBT 100% (PBS 1x with 0.1% Tween-20), MeOH 25% / PBT 75%, MeOH 50% / PBT 50%, MeOH 75% / PBT 25% and 2 washes in MeOH 100%. Lastly, dehydrated embryos were stored at -20ºC, to preserve their RNA content. This dehydration step also makes embryos more permeable to the antibodies during the IMF protocol.

3.2-Immunofluorescence

Immunofluorescence (IMF) is a technique that allows the visualization and location of various components in tissue or cell samples. The detection of these components is achieved by the attachment of specific antibodies to the antigens present in the component in question, the visualization is possible due to fluorophores tagged in the antibodies [65]. Fluorophores are molecules with fluorescent properties, when emitted with radiation of specific wavelength fluorophores absorb this energy and transit from the 'ground state' to the 'excited state', in a few femtoseconds (10^{-15} seconds), afterward they return to their 'ground state' and the remaining energy is released in the form of radiation with a longer wavelength. Using widefield or confocal microscopy is possible to visualize the light emitted from the fluorophore by using a filter cube, that contains barrier filters and a dichroic mirror, this filter cube will permit that the exciting light reaches the sample but only the emitted light reaches the detector of the microscope (Fig. 3.1) [66].

The IMF protocol used in this study was adapted from [67] with the following adjustments: embryos were fixed in 4% PFA at 4ºC overnight (o/n), then dehydrated gradually in a series of MeOH /PBT solutions and stored in 100% MeOH at -20ºC, has described above. Afterward, the embryos were rehydrated gradually in a series of MeOH /PBT solutions and washed twice in PBT for 5 min at room temperature (RT). Then, embryos were submerged in Tris-HCl at pH 9.0 and heated for 5 min at RT followed by 15 min at 70ºC. This additional step to Mateus et al. protocol ensures a better antigen retrieval [68]. Subsequentially, permeabilization using 100% Acetone for 7 min at -20ºC was performed. Next, the embryos were washed in PBT, 1% DMSO, and 1% Bovine Serum Albumin (BSA) and subsequentially blocked in PBT, 1% DMSO, 1% BSA, and 1% Goat serum (GS) (blocking solution) for 2 hours at RT. Embryos were incubated in primary antibody (rabbit anti-PSmad1/5/9, 1:100 (Cell Signaling), diluted in blocking solution at 4ºC o/n. The following day embryos were washed 2 times in PBT, 1% DMSO, and 1% BSA for 5 min and incubated in secondary antibody (Alexa Fluor 568 anti-rabbit, 1:1000) conjugated with DAPI (1:1000) diluted in blocking solution o/n at 4ºC. On the next day, embryos were washed 2 times in PBT, 1% DMSO and 1% BSA for 5 min. Embryos were mounted in 80% Glycerol, 2% DABCO diluted in PBS, and then imaged in Leica SP5II confocal microscope.

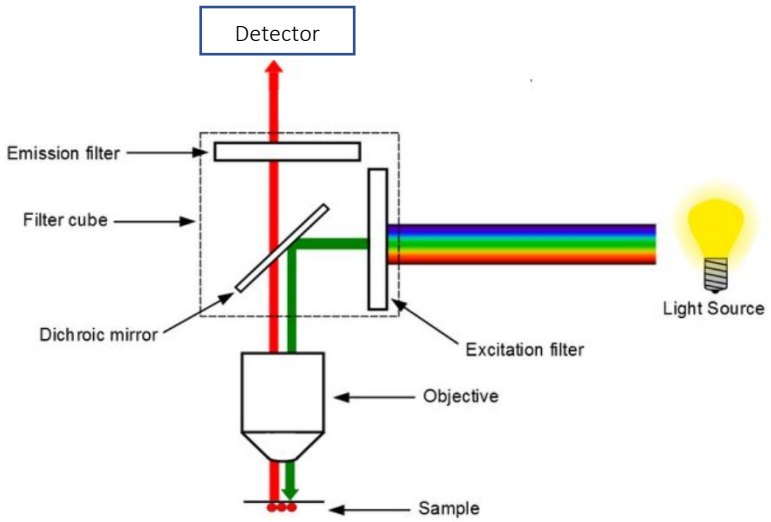

Figure 3.1: Schematic representation of a filter cube. Has the radiation from the light source passes through the excitation filter only the excitation wavelength passes through and is reflected to the sample by the dichroic mirror. Upon being excited by the fluorophores present in the sample, radiation with longer a wavelength is emitted and can pass through the dichroic mirror and be read by the detector. Adapted from [69].

3.3-Real-Time Quantitative Polymerase Chain Reaction (RT-qPCR)

3.3.1-RT-qPCR technique

RT-qPCR is a variant technic of PCR where the detection and quantification, in real time, of PCR products, is possible. This is due to the incorporation of a fluorescent molecule that acts as a reporter [70]. In this study, the fluorophore used was SYBR Green, a cyanine that binds to double-stranded DNA. This technique has three phases of amplification: the growth phase, the exponential phase, and the plateau phase (Fig. 3.2). As the reaction starts, the PCR products start to duplicate, but the level of the signal in this growth phase is too small to distinguish it from the background. After some cycles, the levels of product grow exponentially, until they reach the plateau phase where the amplification reagents start to be scarce and the levels of fluorescence stabilize (Fig. 3.2) [70]. The measurements to study gene expression in this technique are read in the exponential phase, due to being a more accurate representation of the PCR reaction quantification, given that no reagent limitations exist. Gene expression is calculated by comparing the number of amplification cycles necessary to reach a particular threshold level between the gene of interest and a reference gene. The number of cycles necessary to reach this threshold is called CT value (Fig. 3.2). The CT values of both sample and control gene are normalized to the reference gene, generally a housekeeping gene, which has a constant expression. In this study, we used *β-actin2* has the reference gene found to be stably expressed throughout zebrafish development [71]. Both, the gene of interest and the reference gene were measured in triplicate, to have three technical replicates. Afterward, we would perform at least two biological replicates. The raw data was analysed using "Bio-Rad CFX Manager"

program and "Excel" to compile the data and calculate relative gene expression using the $2^{-\Delta\Delta Ct}$ method [70]. The statistical analysis was performed in GraphPad Prism, using Unpaired T-test and ANOVA test to determine statistical significance amongst samples. All the reagents and amplification programs utilized to perform this technique are reviewed in Table 3.1 and 3.2.

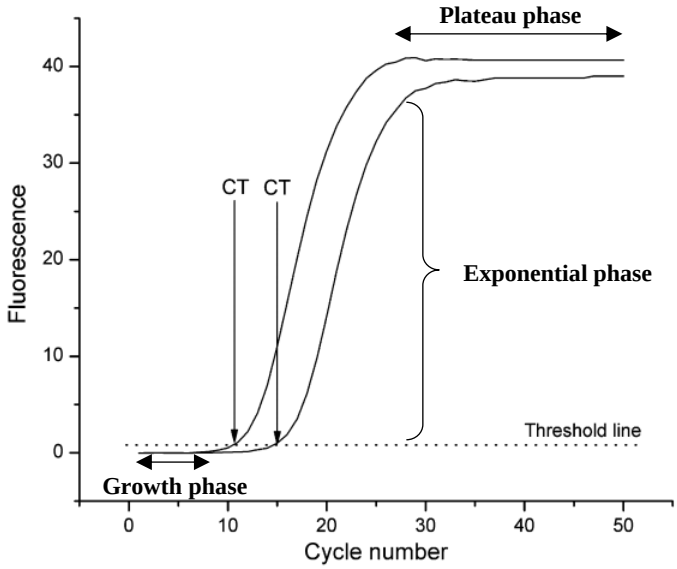

Figure 3.2: Fluorescence progression during RT-qPCR. During RT-qPCR fluorescence signal presents three distinct phases, a growth phase, exponential phase, and plateau phase. A threshold level is placed just above the background signal when the exponential phase begins, CTs are determined by the number of cycles necessary to reach this threshold. Adapted from [70].

Table 3.1: Reagent proportions used in RT-qPCR reaction. Each sample was subjected to RT-qPCR amplification using these volumes. SYBR Green - iTaq™ Universal SYBR® Green Supermix (Bio-rad, USA). FW- forward. RV- reverse. H_2O D|R- DNAse/RNAse treated H_2O.

REAGENTS	VOLUME (µL)
Sybr Green	5
FW Primer	0,5
RV Primer	0,5
cDNA (1:4)	2
H_2O D|R	2
Total	**10**

Table 3.2: RT-qPCR amplification program performed in this study.

	CYCLE 1	CYCLE 2	
Temperature	95ºC	95ºC	62ºC
Time	3 min	10s	30s
Repetitions	1	40	

3.3.2-RNA extraction

To extract RNA to use in RT-qPCR technique, we first dissected the embryos, sectioning the portion with the fins (around 50 fish per condition) at stages 24hpf, 32hpf, 48hpf, 56hpf, 72hpf, 86hpf, 96hpf, and 120hpf. To do so, embryos were dechorionized and anesthetized with tricaine, the dissected pieces were preserved in RNAlater® (Fisher) at -20ºC. Afterward, the samples were homogenized using a rotor-stator homogenizer.

Upon homogenization, samples were centrifuged at 4ºC, 14 000 x rpm, for 1 hour, and the supernatant was discarded. Then 400µL of Trizol was added and the samples were centrifuged at 12000 x g for 2 min at 4ºC, to dissociate nucleoprotein complexes. The samples were incubated at RT for 5min before adding 80µL of chloroform. Next, they were briefly vortexed, incubated for 3 min at RT, and centrifuged at 12000 x g for 15 min at 4ºC. The aqueous phase (containing the eluted RNA) was then transferred to a new tube and the phenolic phase (containing DNA and other cellular compounds) was discarded. Subsequently, 200 µL of isopropanol was added and the samples were incubated for 10 min at RT, followed by centrifugation at 12000 x g for 15 min at 4ºC. The supernatant was discarded, and the pellet was resuspended in 400 µL of ethanol at 75% before being vortexed and centrifuged at 12000 x g for 5 min at 4ºC. Later, the supernatant was discarded, the pellet was resuspended in 150 µL 75% ethanol, vortexed and the previous centrifugation step was repeated. Lastly, the ethanol was removed, and the tubes were left open to dry for 15 min at RT. Afterward, the pellets were resuspended in 25 µL of H_2O DNAse/RNAse free and incubated at 60ºC for 10 min, being briefly homogenized at the 5 min mark.

To remove contaminant DNA, we performed DNAse I digestion, as indicated in table 2.3, incubating the mix at 37ºC for 1 hour, followed by 2 min in ice. After the digestion, RNA precipitation was conducted. To do so, 4µL of sodium acetate 2M pH4.6 were added to the samples to reach a concentration of 0,2M. Then, 200 µL of 100% ethanol was added and the samples left to invocate at -20ºC overnight. On the following day, samples were centrifuged at 10000 rpm, 4ºC for 30 min, then the supernatant was discarded and 150 µL of 75% ethanol was added and the samples were vortexed briefly and centrifuged at 4ºC, 10 000 rpm for 10 minutes. Following this, 150 µL of 75% ethanol was added and the previous centrifugation step was repeated. Afterward, the supernatant was removed, and the samples were left to dry with the lids open for 15 min at RT. Lastly, the samples were resuspended in 25 µL of H_2O DNase/RNase free and the amount of RNA was measured in a NanoDrop machine. The RNA samples were stored at -80ºC until usage.

Table 3.3: DNAse digestion mix. Buffer-10x DNAseI Recombinant RNA-free Incubation Buffer 10x (Roche). DNAse I (Roche). H_2O D|R- H_2O DNAse/RNAse free.

COMPONENTS	VOLUME
RNA Mixture	25 µL
Buffer 10x $MgCl_2$	4 µL
DNase I	1µL
H_2O D|R	10 µL

3.3.3-RNA conversion to cDNA

To perform RT-qPCR analyses, RNA must be converted into cDNA. We performed cDNA conversions using the High-Capacity cDNA Reverse Transcription Kit (Applied Biosystems, Vilnius, Lithuania), by which 500 ng of RNA from each sample were converted into cDNA using the mix in table 3.4 and following the thermocycler program indicated in Table 3.5.

Table 3.4: Reagents used to convert RNA into cDNA.All reagents were used from the High-Capacity cDNA Reverse Transcription Kit (Applied Biosystems, Vilnius, Lithuania) except for the Ribolock RNase inhibitor. H_2O D|R- H_2O DNAse/RNAse free.

COMPONENTS	VOLUME
RNA / H_2O D|R	10 µL
Buffer 10x	2 µL
25X dNTP	0,8 µL
10X Random Primers	2 µL
Multisense 20X	1 µL
Ribolock RNase inhibitor	0,5 µL
H_2O D|R	3,7 µL

Table 3.5: Thermocycler program used in RNA conversion to cDNA.

TEMPERATURE (ºC)	TIME (MIN.)
25	10
37	120
85	5
4	Until removal

To confirm cDNA products quality, PCR validations were performed using *β-actin2* primers (Table 2.6) and H_2O DNAse/RNAse free was used as a negative control. The thermocycler program is indicated in table 3.7. To confirm the results, the amplified samples were loaded on a 2% agarose gel that was prepared by dissolving 1g of electrophoresis grade agarose (NZYtech, Portugal) in 50 mL of Tris-Acetate-EDTA (TAE) 1x. The solution was heated to dissolve faster, followed by a cooling down and the addition of 2µL of Green Safe Premium (NZYtech, Portugal). The mixture was then poured into a mold to solidify. Once the gel became solidified, the samples and a 1 kilobase (Kb) ladder (Solis Biodyne) were loaded and the gel was run in 1X TAE buffer at 100 V. To reveal the electrophoresis products, ultraviolet spectroscopy (Molecular Imager ® Gel Doc ™ XR+ Imaging System, Bio-Rad, USA) was used.

Table 3.6: Reagents used for validation PCR to confirm cDNA synthesis. Master mix- NZYTaq II 2x Green Master Mix, NZYtech, Lisbon, Portugal. FW- forward. RV- reverse. H_2O D|R- DNAse/RNAse treated H_2O.

COMPONENTS	VOLUME (ML)
Master Mix	5
FW Primer	0,5
RV Primer	0,5
cDNA	0,3
H_2O D|R	3,7

Table 3.7: Thermocycler program used in for validation PCR to confirm cDNA synthesis.

	Cycle 1	Cycle 2			Cycle 3	Cycle 4
Temperature	95ºC	95ºC	72	72ºC	72ºC	4º C
Time	3 min	30s	30s	1 min	5 min	Until removal
Repetitions	1		30		1	----------

4-RESULTS

4.1-BMP-signaling during fin development relates to finfold size

4.1.1-BMP-signaling in embryonic finfolds

The goal of this study was to evaluate the molecular pathways involved in the formation of three different-sized embryonic finfolds in the zebrafish lines *wild-typeAB (wtAB)*, transgenic *hsp70:hoxd13a* (*hoxd13a*+++), and mutant *leo*^{d1}*/lof*^{dt2}. Previous data from our lab demonstrated that the transgenic line overexpressing *hoxd13a* has a shortening of the finfold and expresses higher levels of *bmp2b* than its counter partner *wtAB*, whereas the mutant *leo*^{d1}*/lof*^{dt2} shows the opposite tendency: elongation of the finfold and lower expression of *bmp2b* than the wild-type condition [62]. However, given that Bmp proteins are diffusible molecules, their expression may not accurately reflect where their action takes place. To gain insight into this question, we performed IMF analyses at particular developmental stages in the three zebrafish lines mentioned above. To specifically target the BMP-signaling, we used p-Smad1/5/9 antibody, given that upon activation of this pathway, the R-Smad proteins within the cytosol become phosphorylated.

At a first glance, we observed that the majority of the BMP-signaling occurring in the fins is in the embryonic finfold between stages 56hpf and 86hpf, being this trend present in all conditions and stages analysed (Fig. 4.1). As previously demonstrated, at 56hpf the finfold of the mutant *leo*^{d1}*/lof*^{dt2} is already significantly enlarged than the finfold of the *wtAB* [62] (Fig. 4.1 A-B). In the *wtAB* finfold we observed more signal intensity than in the mutant's longer finfolds and this tendency is maintained at 86hpf (Fig. 4.1 D-E and .4.1 G-H). Regarding the transgenic line *hoxd13*+++, we observed a drastic reduction of the finfold size, in comparison with the *wtAB* condition, at 56hpf (Fig. 4.1 A,C) and 86hpf (Fig. 4.1 E,F) and we could observe that the shorter finfolds presented more compacted cells with BMP-signaling activity, particularly visible at 86hpf (Fig. 4.1 C,F). We were, however, unable to find significant differences with our intensity analyses for this particular line (Fig. 4.1 G-H).

Our data suggest that shorter finfolds relate to higher BMP-signaling activity while longer finfolds associate with reduced BMP-signaling activity. Thus, the shortening of the finfold that occurred during vertebrates' evolution might have been due to an increment of the BMP-signaling due to the rising expression of *hoxd13*, among other genes.

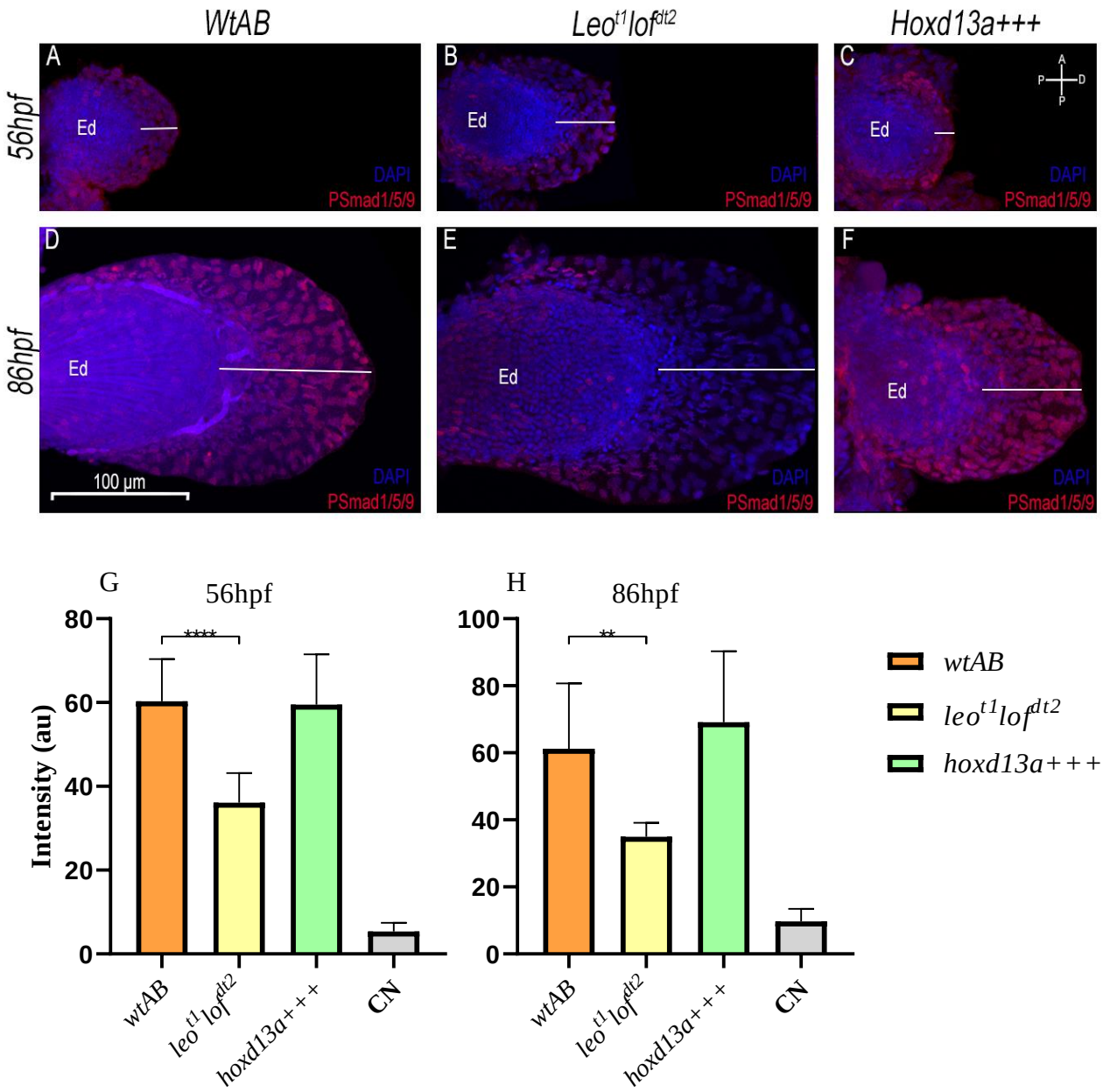

Figure 4.1: BMP-signaling during fin development in *wild-type* (*wtAB*), long finfold mutant (*leo^{t1}/lof^{dt2}*) and transgenic zebrafish overexpression *hoxd13a* (*hoxd13a*+++). (A-C) IMF for p-Smad1/5/9 in *wtAB*, *leo^{t1}/lof^{dt2}* and *hoxd13a*+++, at 56hpf. Note that the *leo^{t1}/lof^{dt2}* condition already presents a longer finfold at 56hpf. (D-F) IMF for p-Smad1/5/9 in *wtAB*, *leo^{t1}/lof^{dt2}* and *hoxd13*+++ at 86hpf. Note that the *leo^{t1}/lof^{dt2}* presents less signaling activity in the finfold, in both 56hpf and 86hpf, in comparison with the other lines, in which the signal is more prominent in the finfold (especially in the *hoxd13a*+++ condition). (G-H) Signal intensity in the finfold of the three lines at 56hpf and 86hpf. Note that at 56hpf the *leo^{t1}/lof^{dt2}* fins show less signaling activity than the *wtAB* fins (*wtAB* n=9, *leo^{t1}/lof^{dt2}* n=12, *hoxd13*+++ n=3, CN n=3, ****p < 0.0001), and the same is observed at 86hpf (*wtAB* n=9, *leo^{t1}/lof^{dt2}* n=8, *hoxd13*+++ n=6, CN n=3 **p < 0.01). No statistical differences were detectable in the analyses between the *wtAB* and the *hoxd13a*+++ conditions. Each column represents the mean ± SD. Statistical significance evaluated by unpaired t-test. Ed-Endoskeleton disk. CN-Negative Control. Top right cross indicates fin orientation. White line over fins represents finfold length. Scale bar is 100 µm.

4.1.2:*bmp2b* expression dynamics during fin development

Throughout tetrapod limb development BMP activity fluctuates, as seen in a study conducted by Pignatti and colleagues [56]. These authors detected that, during mouse early limb development, BMP activity is high and important for the establishment of the AER and then decreases, which is associated with the patterning of the limb bud. In later phases, the BMP activity rises again, which is thought to signal the cells' transition to chondrogenesis. Taken into consideration the detection of variations in the BMP signaling during the development of the finfold in the different zebrafish lines analysed (*wtAB, hoxd13a+++, leo*^{d1}*/lof*^{dt2}*)*, we next asked which components of this pathway have differential expression and how is their dynamics throughout development in these distinct genetic backgrounds.

To this end, we generated a cDNA library from fins dissected at different developmental stages, in all three lineages, and we performed RT-qPCR analyses for a variety of genes involved in the BMP-signaling pathway. Given that the main focus in this study was to evaluate finfold development, we initiated the analyses at 32hpf, the stage previous to the AER-to-AF transition in zebrafish (34-36hpf) and in which the endoskeleton primordia is already formed [29], Moreover, most genes analyzed during this work were described to be silenced in the endoskeleton and active in the finfold after 32hpf [72] and therefore, we assumed that most of the differential dynamics found in BMP-signaling components were primarily connected to finfold development.

Our findings revealed that *bmp2b* has a dynamic expression pattern throughout finfold development, which varies between lines (Fig. 4.2). In the *wtAB*, *bmp2b* expression tends to decrease over time, showing a subtle peak of expression at 24hpf, followed by a slight decrease until 48hpf and a second subtle peak of expression at 72hpf. After that, the expression drops at 86hpf and remains stable until 120hpf (Fig. 4.2 A). We hypothesized that the first peak may be associated with the transition of the AER into the finfold, and the following decrease in expression might be associated with a stage where the patterning mechanism of the finfold cells occurs. The second peak of expression, at 72hpf may relate to a stage in which cells are exiting towards differentiation, similarly to what has been reported during chondrogenesis in tetrapods [56]. More studies will need to be done to further address this hypothesis. The same downward trend in *bmp2b* expression was observed in the *leo*^{t1}*/lof*^{dt2} fins, but only after 48hpf (Fig. 4.2 B), which suggests a delay in the BMP-signaling dynamics in the mutant condition. When compared to *wtAB* fins, the levels of expression tend to be overall lower in the mutant with longer finfolds, as we hypothesized in [62] (Fig. 4.3A).

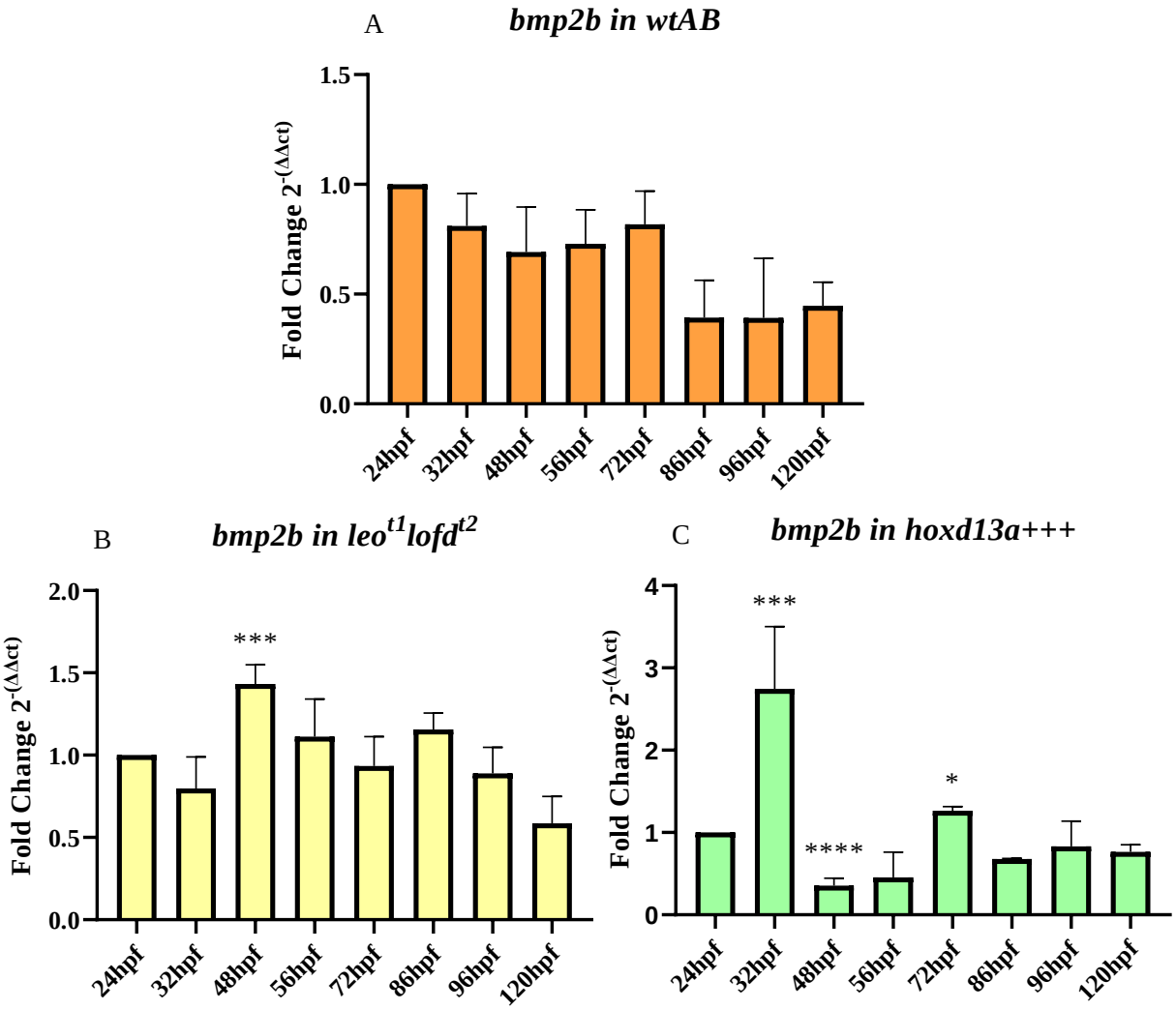

Figure 4.2: *bmp2b* expression dynamics. Gene expression was evaluated by RT-qPCR throughout fin development. (A) *bmp2b* expression in *wild-type* (*wtAB*). Note that the expression of *bmp2b* in the *wtAB* has a decreasing trend throughout fin development with two subtle expression peaks, one at 24hpf and another at 72hpf. (B) *bmp2b* expression in the mutant line with longer finfolds (*leo*^{t1}/*lof*^{dt2}) showing the same downward trend, however just after 48hpf. (C) *bmp2b* expression in the transgenic line with shorter finfolds *(hoxd13a+++)* revealed a peak of expression at 32hpf, after the induction of *hoxd13a* overexpression by heat-shock. Each column represents the mean ± SD. The fold change for each line is normalized to its specific 24hpf stage. Differential expression was evaluated between a designed stage and the previous one using one-way ANOVA test and the statistical significance is indicated with asterisks (*p < 0.05, ***p < 0.001, ****p<0.0001).

Regarding the transgenics overexpressing *hoxd13a*, we observed a great peak of expression at 32hpf (Fig. 4.2 C), just after the first heat-shock, reinforcing the hypothesis that the hoxd13a transcription factor triggers the expression of *bmp2b* which potentiates the finfold truncation [62]. Contrary to what was expected, the levels of expression afterward drop significantly (Fig. 4.2 C) and are lower compared to the *wtAB* (Fig. 4.3 B). We suggest that the rapid increment of *bmp2b* expression at 32hpf triggered compensatory mechanisms to attenuate the molecular effects of the *hoxd13a* overexpression with the aim to keep the normal levels of *bmp2b* expression. However, given that the heat-shock treatments were continuously administered, the expression of *bmp2b* increased again reaching levels similar to the *wtAB* at later stages (Fig. 4.3 B).

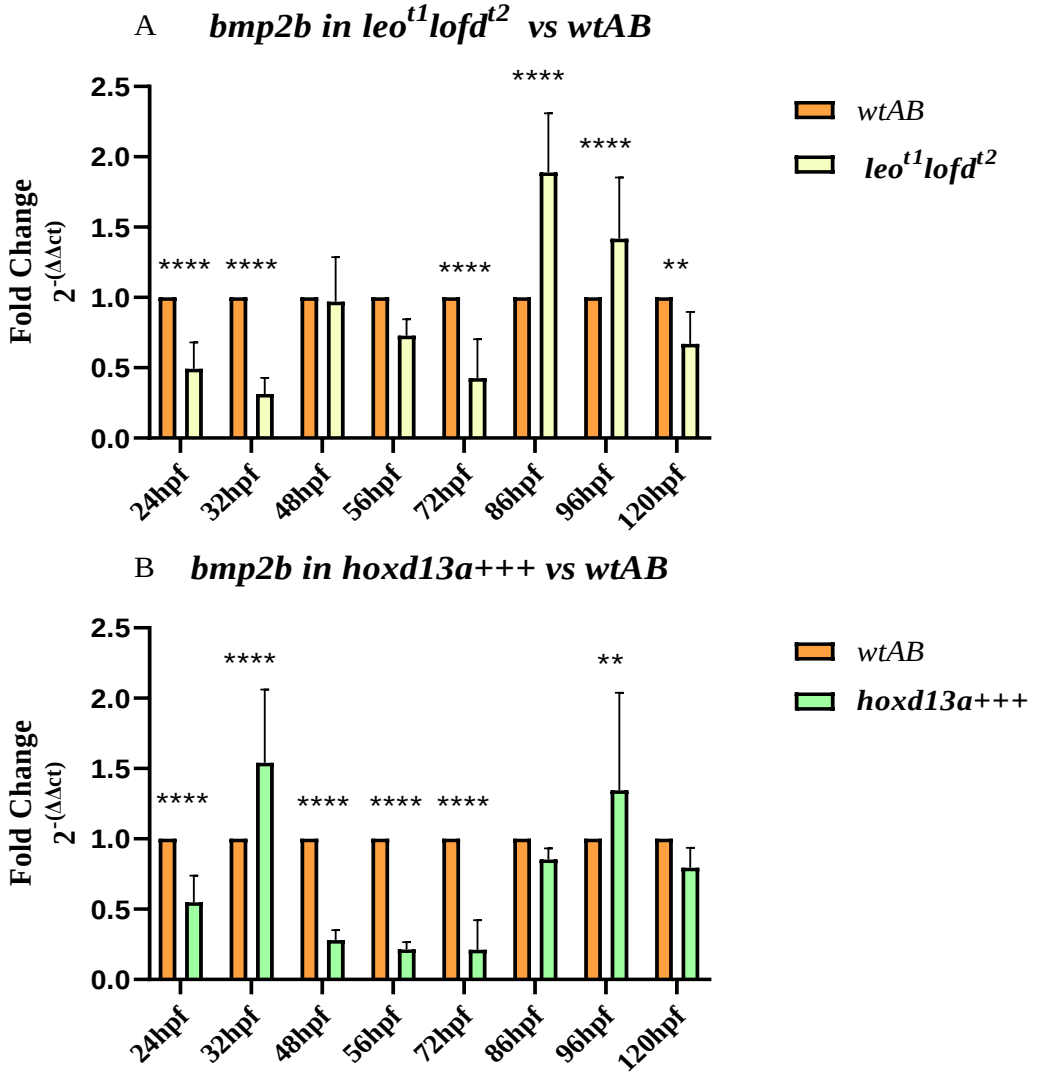

Figure 4.3: Comparison of *bmp2b* expression in different zebrafish lines. Expression was evaluated by RT-qPCR throughout fin development. (A) Comparison of *bmp2b* expression between wild-type (*wtAB*) and *leo*^{t1}/*lof*^{tl2} with longer finfolds. Note that the mutant line has an overall lower expression, except in later stages. (B) Comparison of *bmp2b* expression between wild-type (*wtAB*) and *hoxd13a*+++ transgenic line. Note higher expression levels at 32hpf in the transgenic, due to the heat shock, and afterward, the levels diminish drastically. Each column represents the mean ± SD. For each stage, the fold change was normalized to the *wtAB* fold change. Differential expression for each stage was normalized to *wtAB* of the corresponding stage using two-way ANOVA test with multiple comparisons and the statistical significance is indicated with asterisks (*p < 0.05, **p<0.01***p < 0.001, ****p<0.0001).

4.2. Expression of other BMP-signaling pathway molecules

4.2.1 *smad1*

BMP-signaling pathways involve many molecules that greatly influence its regulation, from antagonists and agonists that control BMP progression in the extracellular niche, to cytosol proteins that partake important roles in BMP-signaling transduction [60]. As seen in the IMF analyses, the BMP-signaling in the finfold differs in the zebrafish lines analyzed. When we compared the *wtAB* and the *leo*^{d1}*/lof*^{dt2} conditions, we observed a significant reduction in the BMP-signaling in the long finfold mutants at 86hpf. However, upon looking at the expression dynamics of *bmp2b*, we obtained contrasting results at 86hpf indicating higher expression in the mutants. These results suggest that the expression of *bmp2b* on its own is insufficient to explain the fluctuations in the BMP-signaling throughout fin development and other components of this pathway should be also analyzed in the three-selected lines.

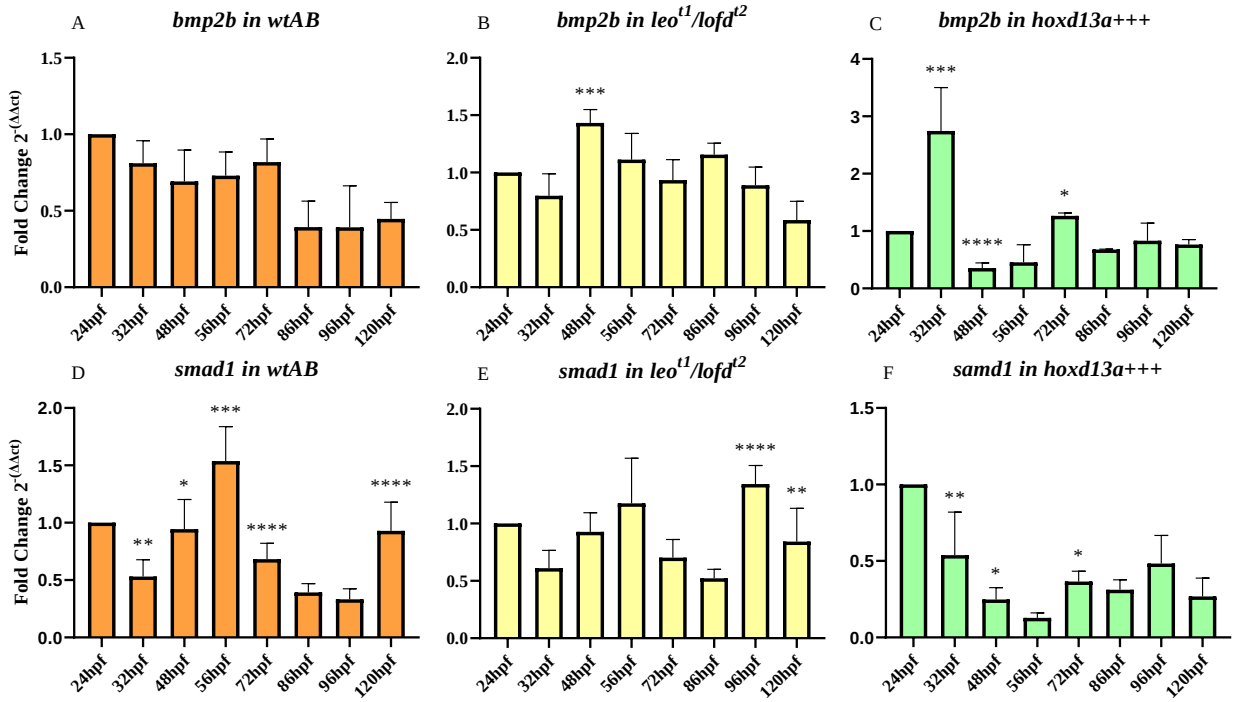

Figure 4.4: Expression dynamics of *bmp2b and smad1*. Gene expression was evaluated by RT-qPCR throughout fin development. (A-C) Expression of *bmp2b* in *wtAB*, *leo*^{t1}*/lof*^{dt2} and *hoxd13a+++*. (D) *smad1* expression in *wild-type* (*wtAB*). Note the fluctuation of *smad1* expression throughout fin development with expression peaks at 56hpf and 120hpf. (E) *smad1* expression in *leo*^{t1}*/lof*^{dt2} mutants with longer finfolds. Note similar expression dynamics in comparison with the *wtAB* condition. (F) *smad1* expression in the *hoxd13a+++* transgenics with shorter finfolds. Note distinct dynamic in comparison with the other lines analyzed. Each column represents the mean ± SD. The fold change for each line is normalized to its specific 24hpf stage. Differential expression was evaluated between a designed stage and the previous one using one-way ANOVA test and the statistical significance is indicated with asterisks (*p < 0.05, ***p < 0.001, ****p<0.0001).

One of these molecules is SMAD1, encoded by the *smad1* gene, a R-SMADS protein involved in the cytoplasmic part of the BMP-signaling pathway (Fig. 1.8) [56]. To evaluate how *smad1* expression variations may relate with the differential levels of BMP-signaling observed in the three distinct zebrafish lines, we performed RT-qPCR using the cDNA collections produced from fins at distinct developmental stages (Fig. 4.4).

Comparison of *smad1* and *bmp2b* expression throughout fin development revealed very distinct expression dynamics (Fig. 4.4 A, D). While *bmp2b* expression gradually diminished (Fig. 4.4 A) *smad1* expression fluctuated, presenting peaks of expression at 56hpf and 120hpf (Fig. 4.4 D). In contrast, in the *leo*^{t1}*/lof*^{dt2} mutants, the expression dynamic of *bmp2b* and *smad1* is more related (Fig. 4.4 B, E). In addition, the expression of *smad1* in *wtAB* and *leo*^{t1}*/lof*^{dt2} mutants is also quite similar, with subtle differences in the peaks of expression (Fig. 4.4 D, E). For example, the latest expression peak occurred at 96hpf in the *leo*^{t1}*/lof*^{dt2} mutants while in the *wtAB* occurred at 120hpf (Fig. 4.4 D, E). Interestingly the expression levels were much higher at this stage in the *leo*^{t1}*/lof*^{dt2} mutants than in the *wtAB* (Fig. 4.5 A).

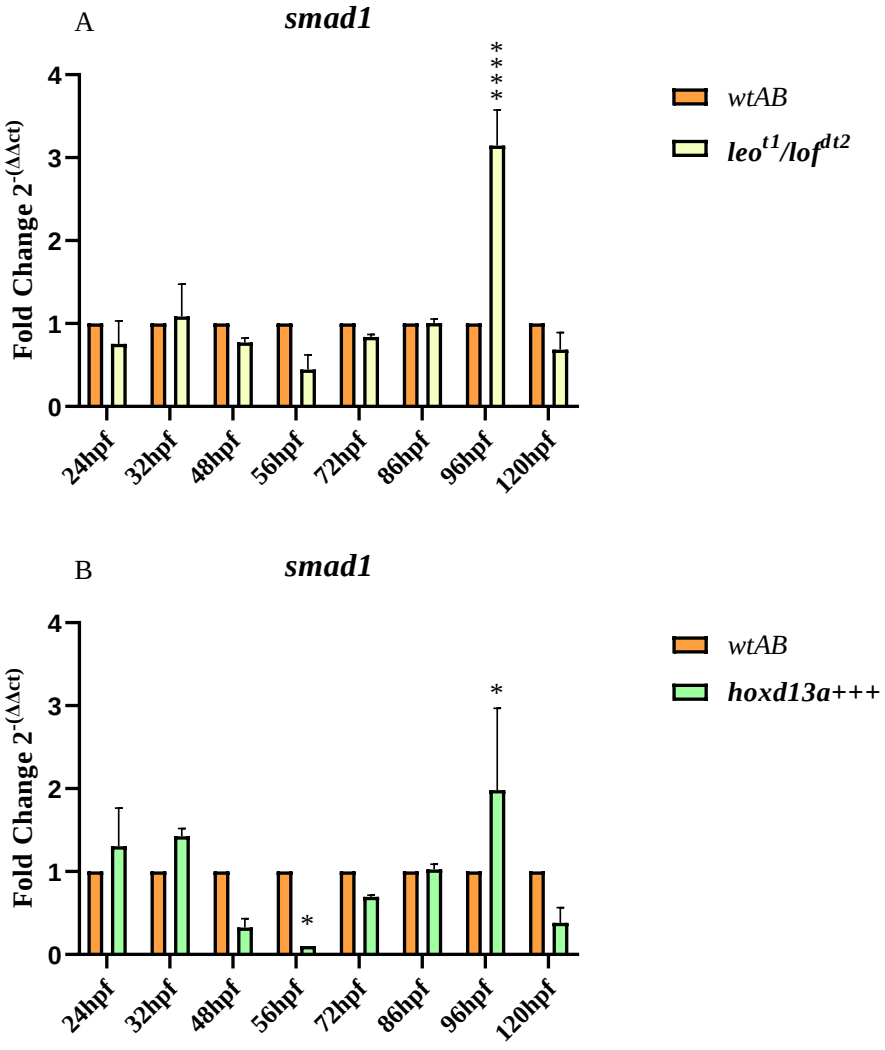

Figure 4.5: Comparison of *smad1* expression in zebrafish lines with distinct finfold size. Expression was evaluated by RT-qPCR throughout fin development. (A) Comparison of *smad1* expression in the wild-type (*wtAB*) and *leo*^{t1}*/lof*^{dt2} with longer finfolds. Note that *wtAB* and *leo*^{t1}*/lof*^{dt2} have similar expression trends but at stages 48hpf and 56hpf the expression is lower in the mutant condition while at 96hpf the expression is higher. (B) Comparison of *smad1* expression in *wtAB* and *hoxd13a*+++ transgenics. Note visible downregulation of *smad1* in the transgenics after the heat-shock treatment (48hpf and 56hpf). Each column represents the mean ± SD. Differential expression for each stage was normalized to *wtAB* of the corresponding stage using two-way ANOVA test with multiple comparisons and the statistical significance is indicated with asterisks (*p < 0.05, ****p<0.0001).

Regarding the transgenic line, we observed similarities in the expression dynamics of *bmp2b* and *smad1* (Fig. 4.4 C, F). Similarly, to *bmp2b*, *smad1* expression dropped at 56hpf and then increased again at 72hpf (Fig. 4.4 C, F). However, while the expression of *bmp2b* drastically increased at 32hpf, as a result of *hoxd13a* overexpression, *smad1* diminished (Fig. 4.4 C-F). These fluctuations can be due to compensatory mechanisms that may have been triggered by the first heat-shock leading to the overexpression of *hoxd13a*. The increment of *bmp2b* expression may have potentiated the activation of mechanisms that then attenuated the BMP-signaling pathway, namely by reducing the expression of some of its fundamental components, such as *smad1*. Surprisingly, the comparison of *smad1* expression levels in *wtAB* and *hoxd13+++* was very similar with the one performed for *wtAB and* leo^{t1}/lof^{dt2} (Fig. 4.5 A-B): *smad1* expression was lower in the *hoxd13+++* and leo^{t1}/lof^{dt2} conditions at 48hpf and 56hpf and higher at 96hpf.

4.2.2 *smoc1* and *smoc2*

Secreted modular calcium-binding protein-1 (SMOC1) and -2 (SMOC2) are matricellular proteins associated with the basement membranes [73, 74]. These proteins can act both as BMP antagonist, by preventing SMAD1/5/8 from being phosphorylated by the type I-receptor (Fig. 1.8), and as expanders of the BMP-signaling gradient, by binding to heparan sulfate proteoglycans (HSPGs) within in the extracellular matrix, which restricts BMP diffusion [61, 67]. In zebrafish, *smoc1* promotes the expansion of BMP-signaling in the developing fin, allowing the gradient to scale with the size of the fin [67]. This is possible due to a feedback loop between BMP and *smoc1*, in which *smoc1* is expressed at the end of the gradient and promotes its expansion towards it, while simultaneously *smoc1* is repressed by the BMP-signaling, maintaining the gradient stable. The authors found that *smoc1* acts primarily in the anterior margin of the fin and postulated that *smoc2* covers the same role in the posterior margin [67].

In our study, we found that the expression dynamic of *smoc1* in the *wtAB* correlates with the one found for *bmp2b* (Fig. 4.6 A, D). Regarding the expression of *smoc2*, the same trend was detected with the exception that the peak of higher expression shifted to 86hpf, instead of 72hpf (Fig. 4.6 A, D, G). When looking at the leo^{t1}/lof^{dt2} mutants, the expression dynamics of *smoc1* exhibited the same heterochronic shifts in expression, as detected for *bmp2b*, having peaks of expression at 48hpf and 86hpf (Fig. 4.6 A, E). Interestingly, *smoc2* presented the highest expression levels at 32hpf, when its paralog *smoc1* had the lowest expression levels (Fig. 4.6 E, H). In addition, the expression of *smoc2* was overall higher in the mutant condition than in the *wtAB* (Fig. 4.7 A, B).

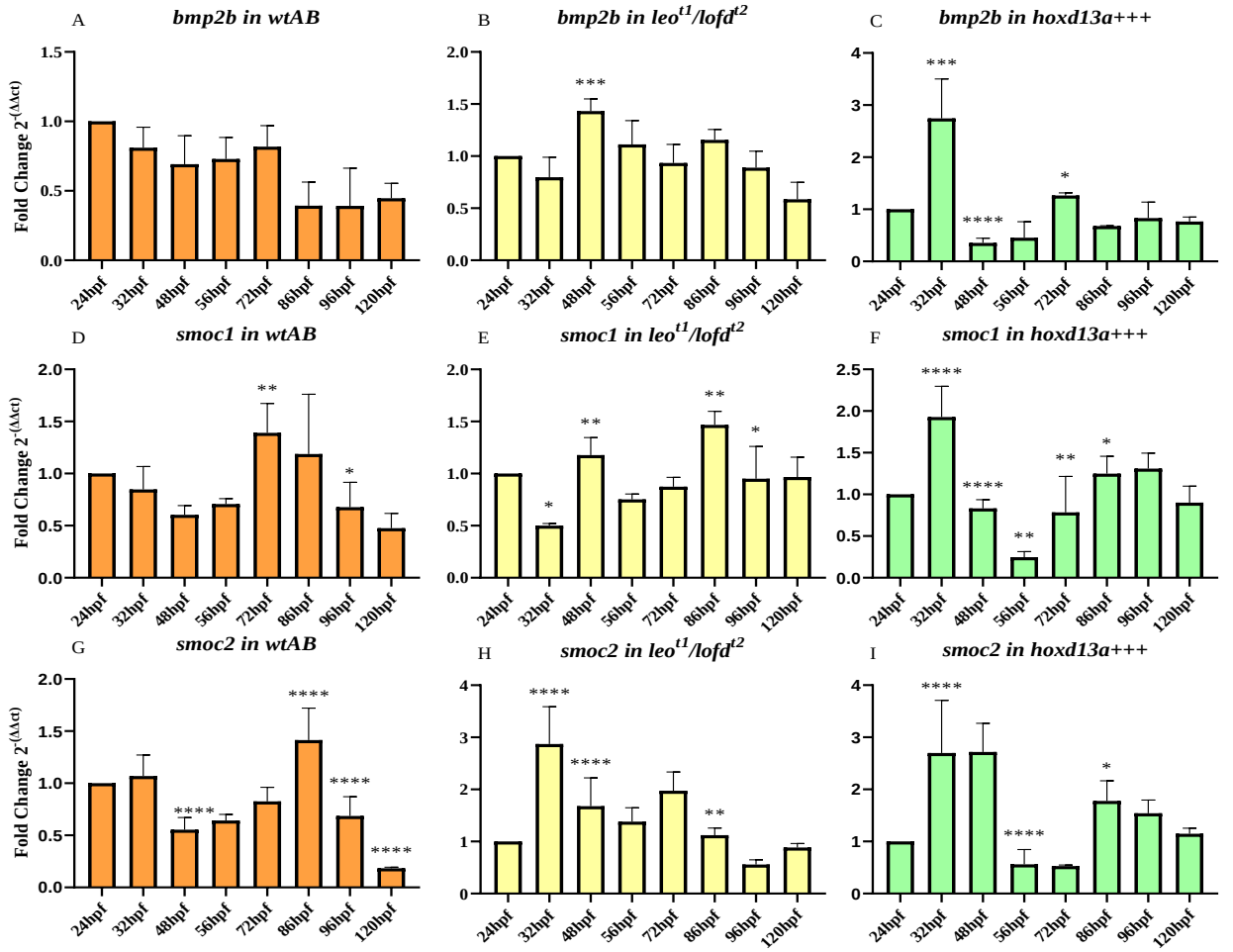

Figure 4.6: Expression dynamics of *bmp2b, smoc1 and smoc2*. Gene expression was evaluated by RT-qPCR throughout fin development. (A-C) Expression of *bmp2b* in *wtAB leo*^{t1}*/lof*^{dt2} and *hoxd13a*+++ lines. (D-F) *smoc1* expression in *wtAB, leo*^{t1}*/lof*^{dt2} *hoxd13a*+++ lines. Note the similarity between the expression dynamics of *bmp2b* and *smoc1*. (G-I) *smoc1* expression in *wtAB, leo*^{t1}*/lof*^{dt2}*, hoxd13a*+++ lines. Each column represents the mean ± SD. The fold change for each line is normalized to its specific 24hpf stage. Differential expression was evaluated between a designed stage and the previous one using one-way ANOVA test and the statistical significance is indicated with asterisks (*p < 0.05, ***p < 0.001, ****p<0.0001).

Then, in the *hoxd13*+++ transgenic line, a peak of expression was detected at 32hpf, for both *smoc1* and *smoc2*, has detected also for *bmp2b*, and the levels declined afterward (Fig. 4.6 C, F). Similarly, to *bmp2b*, *smoc1* and *smoc2* are downregulated at 56hpf and 72hpf, in comparison to *wtAB* (Fig. 4.7 B, D). We hypothesize that, this increment in the expression of *bmp2b*, *smoc1*, and *smoc2* results from the heat-shock treatment performed to instigate *hoxd13a* overexpression in this line. Then, the expression increased again, presenting subtle peaks of expression at 72hpf for *bmp2b* and *smoc1* and at 86hpf for *smoc2* (Fig. 4.6C, F, I). This result shows that *hoxd13a* influences the expression of *smoc1* and *smoc2* directly or indirectly by modulating networks involved in the BMP-signaling.

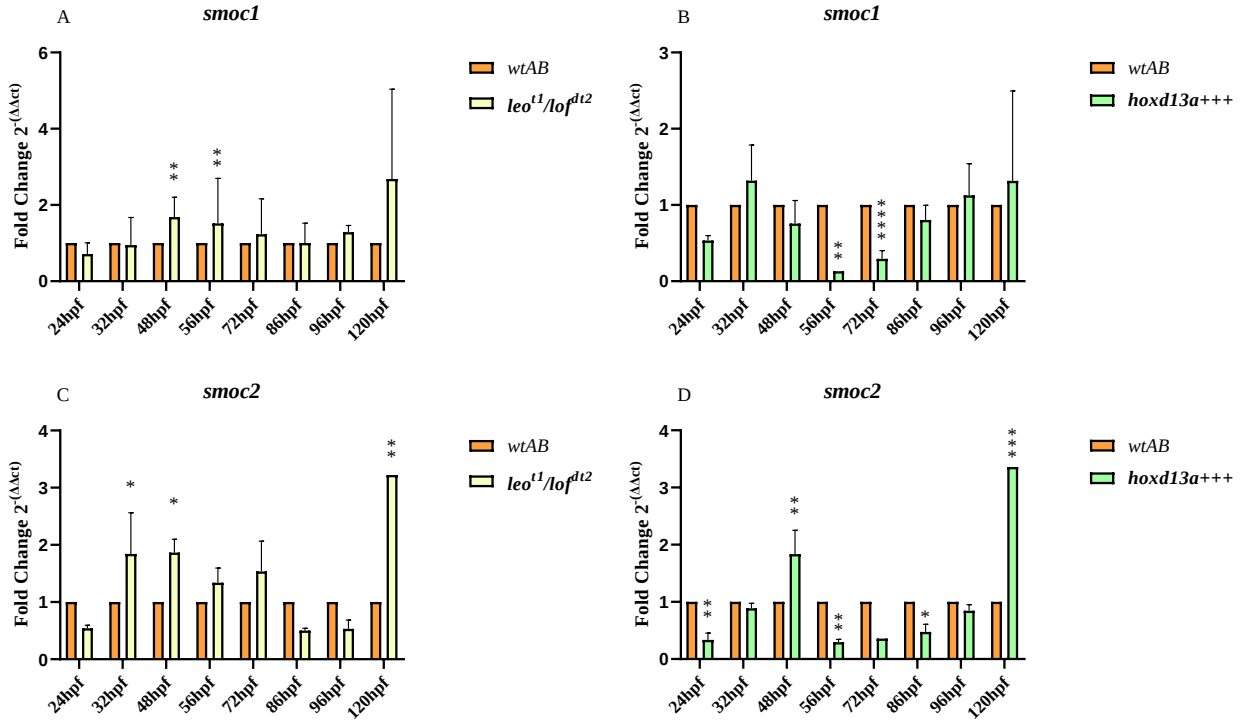

Figure 4.7: Comparison of *smoc1* and *smoc2* expression in different zebrafish lines. Expression was evaluated by RT-qPCR throughout fin development in *wtAB*, *leo*^{t1}/*lof*^{dt2}, and *hoxd13a*+++ lines. (A) Comparison of *smoc1* expression in *wtAB* and longfin mutant (*leo*^{t1}/*lof*^{dt2}). Note that this line present higher levels of expression at 48hpf and 56hpf. (B) Comparison of *smoc1* expression in *hoxd13a*+++ transgenics. Note downregulation of *smoc1* in the transgenic condition in the intermedium stages 56hpf, and 72hpf (C) Comparison of *smoc2* expression in *wtAB* and *leo*^{t1}/*lof*^{dt2}. As *smoc1*, *smoc2* expression tends to be higher in the *leo*^{t1}/*lof*^{dt2} line. (D) Comparison of *smoc2* expression in *wtAB* and *hoxd13a*+++ transgenics. Most stages analyzed exhibit differences in *smoc2* expression. Each column represents the mean ± SD. Differential expression for each stage was normalized to *wtAB* of the corresponding stage using two-way ANOVA test with multiple comparisons and the statistical significance is indicated with asterisks (*p < 0.05, **p<0.01***p < 0.001, ****p<0.0001).

4.2.3 BMP antagonists (*grem1a* and *nogg3)*

BMP antagonists are major players in BMP-signaling regulation [56], being *Gremlin* (*Grem)* and *Noggin* (*Nogg*) the most prominent during limb development [75]. Although both disrupt BMP-signaling by preventing the BMP ligand to reach its receptor, they play different roles in limb development. *Noggin* is required for the formation of the joints and cartilage morphogenesis, whereas *Gremlin* is essential for the maintenance of the AER, participating in the *SHH/GREM1/AER-FGF* feedback loop. In this project, we also investigated the expression of *grem1a*, an ortholog of *Grem1* in zebrafish.

In normal fin development (*wtAB*), we observed that the expression of *grem1a* was, at first, relatively low and then increased in later stages of development, which was particularly evident at 86hpf and 96hpf, when *bmp2b* expression drops (Fig. 4.8 A, D). The mutants *leo*^{t1}/*lof*^{dt2}, in contrast, reached the highest levels of expression earlier (56hpf-72hpf) (Fig. 4.8E). These higher levels of expression may help to explain why at 56hpf and 86hpf these mutants presented lower levels of BMP-signaling (Fig 4.1). In addition, expression level comparisons suggest that a much higher expression of *grem1a* in the longfin mutants at 32hpf and, but not so drastically, at 72hpf and 120hpf (Fig. 4.9 A). Regarding the *hoxd13*+++

transgenics, *grem1a* expression show the highest expression levels later, after 86hpf, when *bmp2b* expression is also higher. This could be a compensatory mechanism allowing the cells to produce more BMP antagonists to lessen the impact of the high levels of BMP. Moreover, *grem1a* expression presented a first subtle upregulation at 48hpf, probably associated with the heat-shock treatment, when *bmp2b* transcripts are higher (Fig. 4.8 C, F). In terms of levels of expression, they seem to be higher in the transgenic condition than in the *wtAB* at those same stages (Fig. 4.9 B).

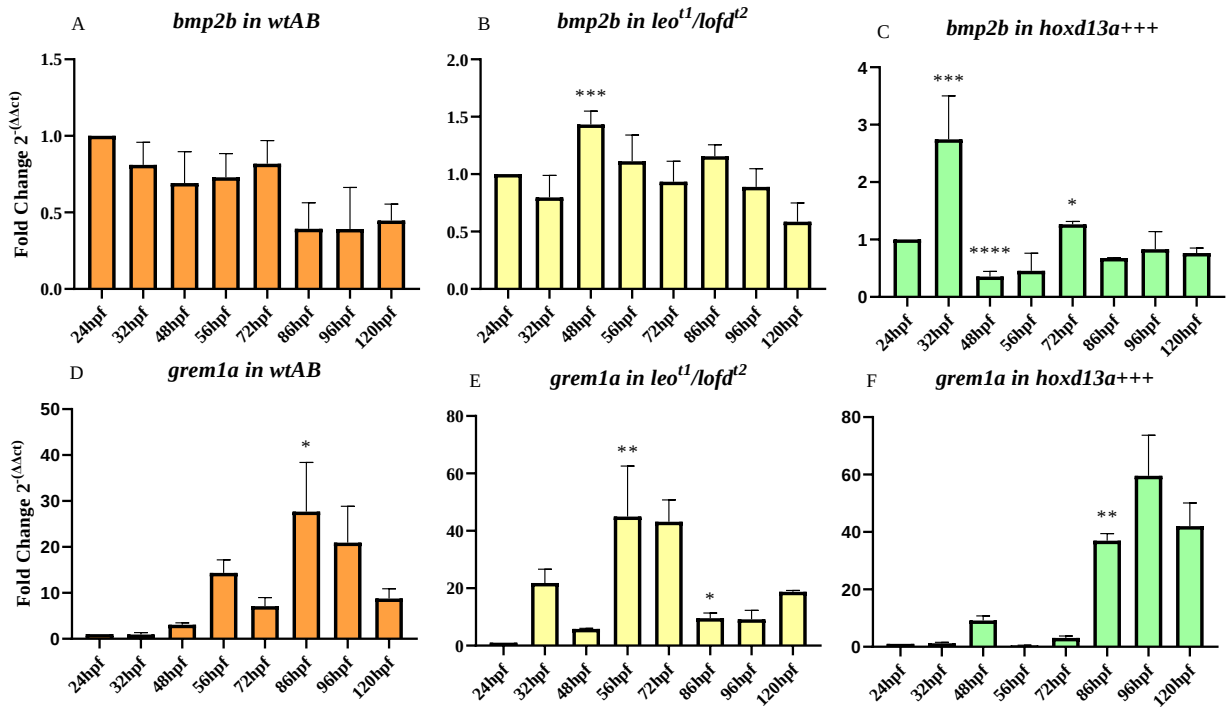

Figure 4.8: Expression dynamics of *bmp2b* and *grem1a*. Gene expression was evaluated by RT-qPCR throughout fin development. (A-C) *bmp2b* expression in *wtAB*, *leo*^{t1}*/lof*^{dt2}, and *hoxd13a*+++ lines. (D) *grem1a* expression in the *wild-type* (*wtAB*). Note peak of expression 86hpf, coincidently with a decrease of *bmp2b* expression. (E) *grem1a* expression in *leo*^{t1}*/lof*^{dt2} mutants. Note peaks of expression at 56hpf and 72hpf, while in the *wtAB* the highest expression levels are detected at 86hpf. (F) *grem1a* expression *in hoxd13a*+++ showing higher levels in the latest stages analyzed. Each column represents the mean ± SD. The fold change for each line is normalized to its specific 24hpf stage. Differential expression was evaluated between a designed stage and the previous one using one-way ANOVA test and the statistical significance is indicated with asterisks (*p < 0.05, ***p < 0.001, ****p<0.0001).

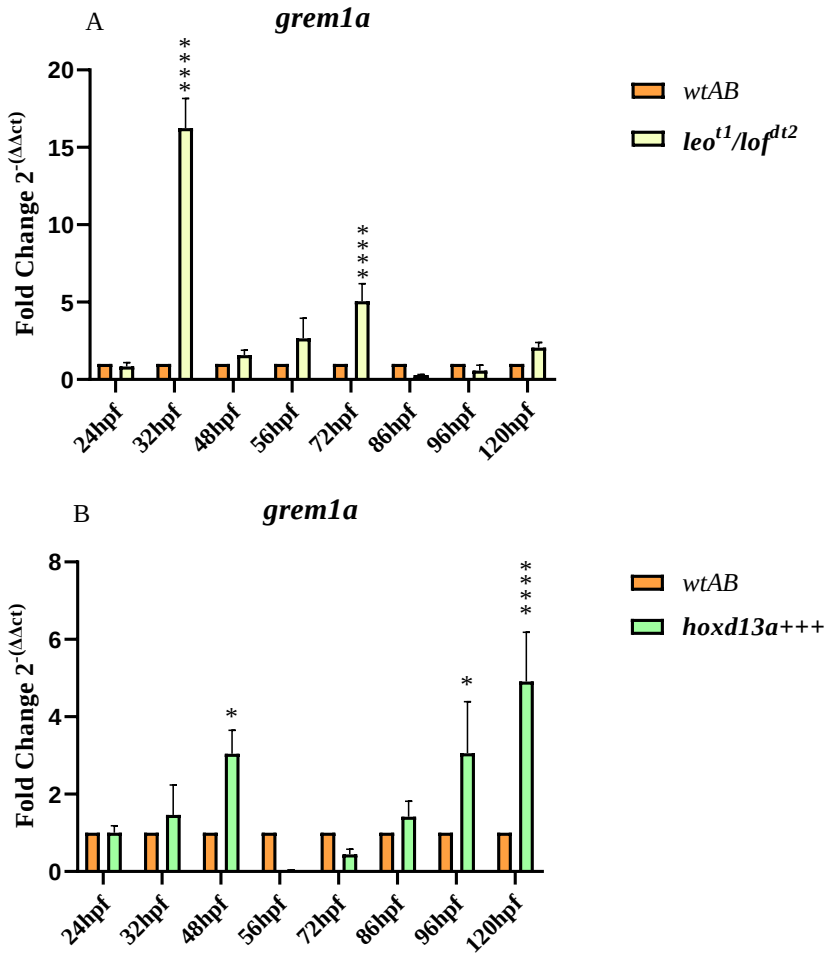

Figure 4.9: Comparison of *grem1a* expression in different zebrafish lines. Expression was evaluated by RT-qPCR throughout fin development. (A) Comparison of *grem1a* expression between *wtAB* and *leo*^{t1}*/lof*^{dt2} with longer finfolds. Note that the mutant shows higher expression at 32hpf and 72hpf. (B) Comparison of *grem1a* expression between *wtAB* and the *hoxd13a+++* transgenic line. Note upregulation of *grem1a* in the latest stages (96hpf and 120hpf). Each column represents the mean ± SD. Differential expression for each stage was normalized to *wtAB* of the corresponding stage using two-way ANOVA test with multiple comparisons and the statistical significance is indicated with asterisks (*p < 0.05, ****p<0.0001).

The other BMP antagonist analyzed in this study was Noggin, which inhibits BMP-signaling the same way as Gremlin [75]. In our analyses, we identified that *bmp2b* and *nogg3* have distinct dynamics of expression throughput fin development in the three lines analyzed (Fig. 4.10 A-E) In the *wtAB* condition, the *nogg3* expression tended to increase up to 96hpf and then progressively diminished (Fig. 4.10 D). The mutant *leo*^{t1}*/lof*^{dt2} also demonstrated a tendency to increase in early stages, however, the peak of highest expression was detected earlier, at 56hpf (Fig. 4.10 F). In addition, further comparisons of the *wtAB* and *leo*^{t1}*/lof*^{dt2} lines brought to evidence what seems to be an advance in the increment of *nogg3* expression in the mutant condition (Fig. 4.11 A). The same trend was also observed regarding *grem1a* expression in this condition, with both genes showing higher levels of expression than *wtAB* in most stages analyzed (Fig. 4.9 A and 4.11 A). In the *hoxd13+++* transgenics *nogg3* expression is higher after 86hpf, when *bmp2b* expression is likewise higher, following the same tendency has *grem1a* (Fig. 4.10 C, E). At the same stages, the transgenic condition appears to have higher levels of expression than the *wtAB* condition (Fig.

4.10 B). Thus, taken together, the expression dynamics of these two BMP antagonists suggests a necessity to block the BMP signaling, which has an impact especially at later stages and may be related with the control of the finfold size.

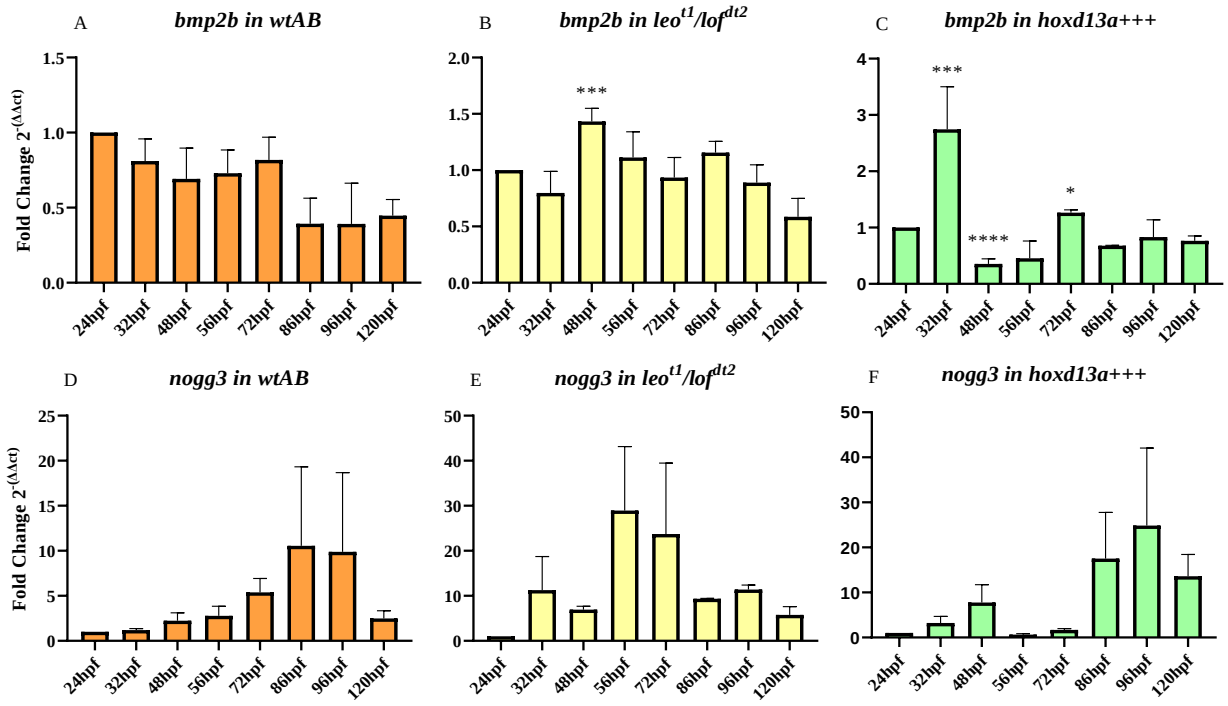

Figure 4.10: Expression dynamics of *bmp2b* and *nogg3*. Gene expression was evaluated by RT-qPCR throughout fin development. (A-C) Expression of *bmp2b* in *wtAB*, *leo*^{t1}/*lof*^{dt2}, and *hoxd13a+++*. (D) *nogg3* expression in *wild-type* (*wtAB*) shows a tendency to increase until 96hpf. (E) *nogg3* expression in *leo*^{t1}/*lof*^{dt2} mutants showing a tendency to increase more abruptly earlier, at 56hpf. (F) *nogg3* expression in *hoxd13a+++* showing higher levels of expression in the later stages, after 86hpf. Each column represents the mean ± SD. The fold change for each line is normalized to its specific 24hpf stage. Differential expression was evaluated between a designed stage and the previous one using one-way ANOVA test and the statistical significance is indicated with asterisks (*p < 0.05, ***p < 0.001, ****p<0.0001).

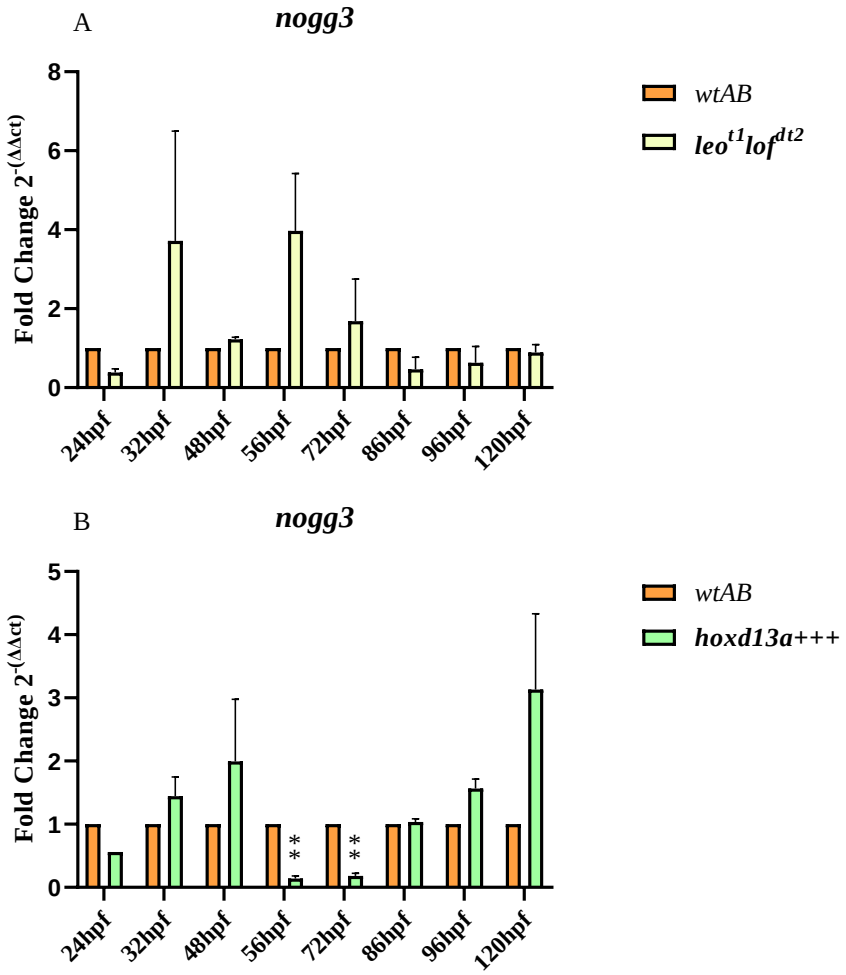

Figure 4.11: Comparison of *noggin3* expression in three zebrafish lines. Expression was evaluated by RT-qPCR throughout fin development. (A) Comparison of *noggin3* expression in *wtAB* and *leo*^{t1}/*lofd*^{t2} lines. Note that the mutant line tends to have a higher level of expression than the *wtAB*, with a decrease at the later stages. (B) Comparison of *nogg3* expression in *wtAB* and *hoxd13a+++* transgenic line. Note *nogg3* downregulation in the transgenic condition at 56hpf and 72hpf. Each column represents the mean ± SD. Expression for each stage was normalized to *wtAB* of the corresponding stage using two-way ANOVA test with multiple comparisons and the statistical significance is indicated with asterisks (**p < 0.01).

4.2.4-*msx2b*

Muscle segment homeobox genes (*Msx*) are known to be targets of the BMP-signaling [76]. Both in invertebrate (*Droshophila*) and vertebrate (*Mus musculus*) BMP signal transduction seems to affect a BMP *cis*-regulatory region in the *Msx2* promoter, which regulates *Msx2* expression [77]. With this in mind, we studied the expression of an ortholog of *Msx2* in zebrafish, known to be expressed during pectoral fin development, *msx2b [78]*.

We found that *msx2b* transcripts start to decline after 32hpf in the *wtAB* condition, while the *bmp2b* expression seemed to be stable up to 72hpf (Fig. 4.12 A, D). The expression dynamics of *msx2b* was,

however, distinct both in the *leo*^{t1}*/lof*^{dt2} and in the *hoxd13a+++* conditions but following the kinetics of *bmp2b* expression (Fig. 4.12 B-C, 4.12 E-F). Interestingly, while in the longfin mutants the peak of highest expression was detectable at 48hpf, in the short finfold transgenics the peak of highest expression was detectable at 32hpf. These results further reinforcing the idea that the mutant line presents a heterochronic shift of the BMP-signaling and that *hoxd13a* overexpression is capable to increment the expression of *bmp2b* and its putative downstream targets, such as *msx2b*. When comparing the expression levels of this gene, we were also able to detect lower expression levels in the mutant condition than in *wtAB* at the earliest stages (Fig. 4.13 A) and an abnormal peak of expression at 32hpf in the *hoxd13+++* transgenics, probably caused by the heat-shock treatment (Fig. 4.13 B).

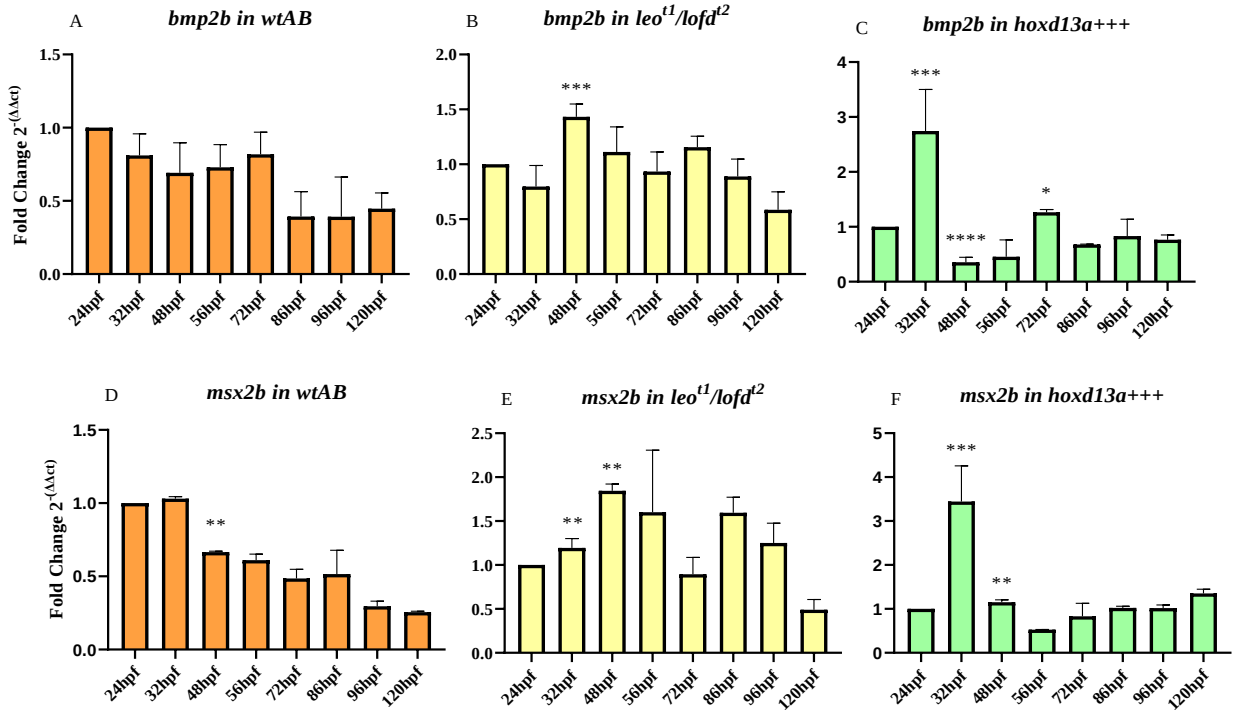

Figure 4.12: Expression dynamics of *bmp2b* and *msx2b*. Gene expression was evaluated by RT-qPCR throughout fin development. (A-C) Expression of *bmp2b* in *wtAB*, *leo*^{t1}*/lof*^{dt2}, and *hoxd13a+++* lines. (D) *msx2b* expression in the *wild-type* (*wtAB*), showing a tendency to decrease throughout development. (E) *msx2b* expression in *leo*^{t1}*/lof*^{dt2} mutants, suggesting that contrary to *wtAB*, the highest expression peaks are at 48hpf and 86hpf. (F) *msx2b* expression in *hoxd13a+++* suggesting that the highest expression peak is at 32hpf. Each column represents the mean ± SD. The fold change for each line is normalized to its specific 24hpf stage. Differential expression was evaluated between a designed stage and the previous one using one-way ANOVA test and the statistical significance is indicated with asterisks (*p < 0.05, ***p < 0.001, ****p<0.0001).

In the *hoxd13a+++* line, we also observed a tendency to higher levels of *msx2b* at the latest stages (96hpf and 120hpf), in comparison with the *wtAB* (Fig. 4.13 B). These results suggest that the overexpression of *hoxd13*, not only influenced the expression of *bmp2b*, but also influenced the action of the BMP-signaling pathway, which culminated with the upregulation of putative targets such as *msx2b*.

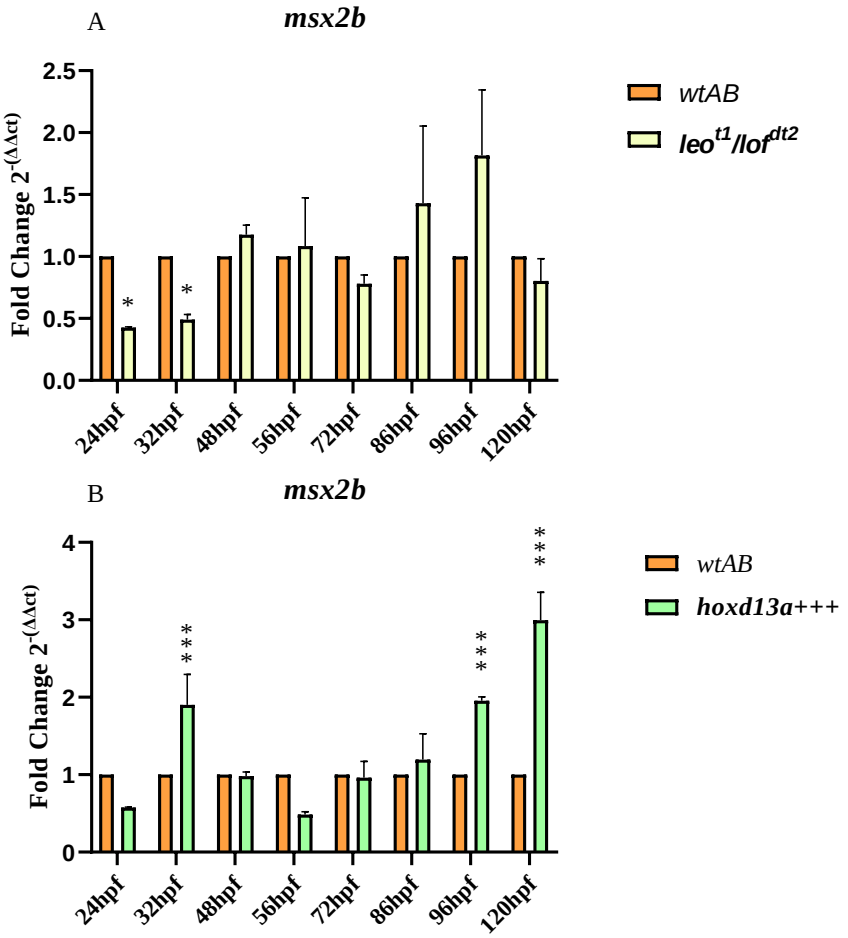

Figure 4.13: Comparison of *msx2b* expression in three zebrafish lines. Expression was evaluated by RT-qPCR throughout fin development. (A) Comparison of *msx2b* expression in *wtAB* and *leo*^{t1}/*lofd*^{t2} mutants showing a similar expression trend. However *msx2b* seems to be downregulated earlier, at 24hpf and 32hpf, in the mutants. (B) Comparison of *msx2b* expression in *wtAB* and *hoxd13a+++* transgenics showing abnormal upregulation of *msx2b* at 32hpf in this latest condition. Each column represents the mean ± SD. Differential expression for each stage was normalized to *wtAB* of the corresponding stage using two-way ANOVA test with multiple comparisons and the statistical significance is indicated with asterisks (*p < 0.05, ***p < 0.001).

5-DISCUSSION

The modulation of *Hoxd13* expression through the elaboration of its enhancer elements has been suggested to be one of the mechanisms involved in the fin-to-limb transition, influencing the development of distal structures, such as the autopod in tetrapod limbs [36]. This transition implicated a progressive increase of endoskeleton elements concomitantly with a reduction of dermoskeleton structures, ultimately leading to limbs with elongated bones and complete absence of dermoskeleton [4]. During zebrafish development, the overexpression of *hoxd13a*, leads to a reduction of the AF, the most distal structure of the embryonic fin in wich the dermoskeleton differentiates, resembling a more limb-like development [36]. Recently, we found that the overexpression of this gene in zebrafish leads to the ectopic expression of several BMPs in the shortened finfold and also when overexpressing *bmp2b*, in the same manner, fins, showed a similar phenotype [62]. With this, a hypothesis emerged suggesting that the *hoxd13a* encoded transcription factor may contribute to the regulation of the finfold size during fin development by inducing the expression of *bmp2b*, which might have been an important mechanisms leading to the fin-to-limb transition.

To further investigate this hypothesis, we characterized how BMP-signaling varies amongst three zebrafish lines with distinct finfold-sizes: *wild-type* condition *(wtAB)*, the long finfold *leo*^{d1}*/lof*^{dt2} condition, and the short finfold *hoxd13a-overexpressing* condition *(hoxd13+++)*. The main goal was to explore how *bmp2b* and other genes implicated in the BMP-signaling may relate with the distinct finfold.

We found that longer finfolds are associated with lower BMP-activity in these structures, has seen when comparing the *wtAB* and *leo*^{d1}*/lof*^{dt2} mutant. Looking at *bmp2b* expression the mutants beside from showing less expression than its wtAB counterpart, the peaks of expression seem to be shifted to later stages in comparison with the *wtAB*. *Leo*^{d1}*/lof*^{dt2} mutants have a mutation in a potassium channel, this mutation may change normal cell electrical balance and therefore influence gene regulatory network [79]. The transcription rate factor is thought to be determined by the absolute value of the cell potential, which is governed by voltage-gated cell ion channels, and the interaction of genetic and electrical signals is expected to offer spatiotemporal information [79]. Considering that RA is known to influence *Hoxd13* expression in the limb bud [80], this differential in charges could disrupt RA activity and delay *hoxd13a* activation. This heterochronic shift would subsequently delay the transcription of *hoxd13a* targets, as *bmp2b* and other BMP-signaling related genes. Indeed, we detected heterochronic shifts in the expression of *bmp2b, and in msx2b*.

Recently Ka et. al 2020 found BMP-signaling to negatively modulate cell proliferation in the ventral fin-fold of zebrafish. Similarly to the pectoral finfolds of *leo*^{d1}*/lof*^{dt2}, when BMP-signaling is inhibited in zebrafish, the ventral finfold extends along the proximal-distal axis [81]. Although paired and unpaired fins emerged in separate evolutionary events, this negative influence of BMP-signaling in cell proliferation in ventral finfold could have been co-opted into pectoral finfold development during evolution. As postulated by Freitas and colleagues [9], most molecular mechanisms responsible for paired fin development were assembled in the finfold of early vertebrates and then coopted to these paired structures.

While our intensity analyses did not show significant differences in BMP-signaling, in the *hoxd13+++* transgenics, we could observe that the shorter finfolds presented more compacted cells with BMP-signaling, specifically at 86hpf. This could be explained by the particular stages where BMP-signaling was measured, since when comparing *bmp2b* expression of *hoxd13+++* with *wtAB* fins, it was found *bmp2b* expression peaks at 32hpf, followed by a downregulation with the expression increasing over the *wtAB* at later stages (starting at 96hpf). Future IMF analysis should be conducted at later stages, to follow these increases of expression and evaluate if the same increment is present in BMP-signaling. Following the findings of Ka et. al 2020 [81], an excess of BMP-signaling could hinder the proliferation of cells within the finfolds, leading to a reduction in size.

These findings support our hypothesis that BMP-signaling modulation was one of the mechanisms by which finfold size was reduced during the fin-to-limb transition. In addition to this, *Bmp2* and *Bmp4* are essential for the maintenance of the AER during mice limb development, and its inhibition results in an elongation of the AER, resembling the AF found in fish fins [63, 82]. In addition, the mechanisms underlying this size-control seem to be conserved to some extent in the AF and AER. However, during fin evolution, the differential expression of genes influencing Bmps expression, such as *Hoxd13*, culminated in a reduction of the AF and maintenance of the AER.

Salsi and colleagues reported that *Bmp2* is a direct downstream target of *Hoxd13* [55], which explains why after the first induction of *hoxd13a* overexpression in the transgenic line *bmp2b* expression levels increased significantly. Interestingly this was not the only gene found overexpressed in response to *hoxd13a* overexpression, *grem1a, msx2b, smoc1, and smoc2* show an upregulation at 32hpf. As none of these genes have been identified as direct downstream targets of *Hoxd13* [55], we hypothesize that the influence of this transcription is indirect, as it happens for *msx2b*, which might be directly controlled by BMP-signaling.

Interestingly some of the genes evaluated in this study have been reported to interact with HOXD13 protein, such as the case of SMAD1. A study conducted in mouse distal limb bud [83] has shown that SMAD1 can act as co-factor of HOXD13, and modulate SMAD-mediated transcriptional activity, without requiring a HOX monomeric DNA-binding capability [83]. This raises the question of weather this HOXD13-SMAD1 interaction is also present during finfold development, implementing another level of regulation in genes related to BMP-SMAD transcriptional activity, such as *msx*.

In regard to the gene expression analyses for *smoc1* and *smoc2*, it was found that these genes tend to have higher expression levels in the leo^{d1}/lof^{dt2} line. This could be due to the lower levels of Bmp transcripts, in an attempt to amplify the BMP-signaling gradient. On the other hand, *Smoc* proteins are also known to be BMP-signaling antagonists [61], and these higher expression values in the mutants may also lessen the BMP-signaling activity in the finfold, which adds to the effect that reduced levels of *hoxd13a* may have on *bmp2b* regulation [62]. Another interesting aspect is that *smoc1* appears to promote outgrowth of the endoskeleton disk of zebrafish fins, by mediating the BMP-signaling gradient [67]. However, as the endoskeleton disc and the fin fold are two markedly distinct structures, it is possible that SMOC proteins may assume different roles in the regulation of the BMP-signaling depending on the cell territory in which they are activated.

In all three zebrafish lines, BMP antagonists *nogg3* and *grem1a* [60] showed a tendency to have a gradual increase of expression up to a certain stage and then start to diminish. However, these peaks of expression vary according to the zebrafish line analyzed. For example, for *gream1a*, the highest peak of expression was detected earlier in the longfin mutants (56hpf) and in the transgenic condition with the shorter finfolds was detected later (96hpf). The same phenomenon was observed regarding *nogg3* expression. However, for this gene, it was not possible to reach statistical significance using only three biological replicates. In addition, it might be necessary to analyze intermediate developmental stages to pinpoint variability within the stages thus far analyzed. Nevertheless, although further analyses are required, our data regarding these two BMP antagonists, suggest that the BMP-signaling is gradually inhibited during fin development and that this process may vary depending on the finfold size. Thus, in the longfin mutants, the BMP-signaling seems to start being inhibited earlier, which corroborates our analyses of psmad1/5/9 expression. This may influence apoptosis and allow further growth of this structure. In contrast, in the short finfold transgenic, the BMP-signaling seems to be inhibited much later, which suggests increased apoptosis associated with finfold truncation.

To further corroborate these results, we also evaluated the expression of a putative downstream target of the BMP-signaling during the development of zebrafish fins from the three distinct lines (*msx2b*). The tetrapod counterpart is involved in interdigital apoptosis during limb development **[**84**]**. In our study, we found that the expression profile of *msx2b* follows a profile related to *bmp2b* expression in all three lines analyzed. This further supports our hypothesis, which we have already begun to investigate **[**62**]**, suggesting that the BMP-signaling may lead to the activation of apoptosis-related genes that then influence finfold size. This could have been the mechanism involved in the finfold truncation during the evolutionary transition from fish fins to tetrapod limbs. This mechanism by which BMP-signaling, regulated by *hoxd13*, increases the apoptotic levels inhibiting finfold elongation, could have been later co-opted in tetrapods, to promote the apoptosis required for the patterning of the digits.

6-CONCLUSION

This work allowed a deeper understanding of the molecular mechanisms associated with the definition of finfold size in zebrafish, namely how *hoxd13* expression levels may influence the BMP-signaling and the expression of the components involved in this network.

Our findings contributed to characterize fin development in the mutant *leo*^{d1}/*lof*^{dt2} line, which to our knowledge has not yet been approached. We found that the expression of the putative *hoxd13a* target, *bmp2b*, is downregulated in this line, and consequently, the fins tend to have inhibited BMP-signaling. Further gene expression analyses of other components of the BMP-signaling corroborated this idea.

We also noted that the expression of several components of the BMP-signaling is post noted a few stages in the longfin mutant in comparison with the other lines analyzed, meaning that a heterochronic shift in expression might have happened. This could be due to the lesser levels of *hoxd13a* expression in this line, taking more time to achieve certain threshold levels to initiate the same BMP-dynamics present in the *wtAB*, a hypothesis that is worth investigating in future projects.

Our findings also allowed the deeper characterization of the transgenics with short finfolds, allowing the overexpression of *hoxd13a*. We found that the heat-shock treatment caused upregulation of several genes involved in the BMP-signaling including its putative downstream targets (*msx2b*). This supports our theory that Hoxd13 modulation during evolution produced finfold truncation by interfering directly or indirectly with BMP-signaling in the finfold. Interestingly at some developmental stages, *bmp2b* was downregulated in this line and we speculate that compensatory mechanisms are triggered due to the increment of *bmp2b* transcripts.

Thus, overall, we propose that modulation of the BMP-signaling leads to a modulation of the apoptotic rate and influences finfold size. Considering our data, we further propose that the reduction of the finfold size during the fin-to-limb transition might have been mediated by increased expression of *Hoxd13*, promoting higher levels of BMP-signaling, which then upregulated the expression of apoptotic genes distally and lead to a reduction in the finfold size throughout evolution.

7-REFERENCES:

[1] M.C. Davis, The deep homology of the autopod: insights from hox gene regulation, Integr Comp Biol, 53 (2013) 224-232.
[2] T. Miyashita, R. Diogo, Evolution of Serial Patterns in the Vertebrate Pharyngeal Apparatus and Paired Appendages via Assimilation of Dissimilar Units, Frontiers in Ecology and Evolution, 4 (2016).
[3] X.G. Zhang, X.G. Hou, Evidence for a single median fin-fold and tail in the Lower Cambrian vertebrate, Haikouichthys ercaicunensis, J Evol Biol, 17 (2004) 1162-1166.
[4] N. Shubin, C. Tabin, S. Carroll, Deep homology and the origins of evolutionary novelty, Nature, 457 (2009) 818-823.
[5] J. Pieretti, A.R. Gehrke, I. Schneider, N. Adachi, T. Nakamura, N.H. Shubin, Organogenesis in deep time: A problem in genomics, development, and paleontology, Proceedings of the National Academy of Sciences, 112 (2015) 4871-4876.
[6] J.K. Thacher, Median and paired fins, a contribution to the history of the vertebrate limbs., Trans Connect Acad Arts Sci, 3 (1877) 281-310
[7] S.G. Mivart, Notes on the Fins of Elasmobranchs, with Considerations on the Nature and Homologues of Vertebrate Limbs, The Zoological Society of London, 10 (1879) 439-484.
[8] M.F. Balfour, On the development of the skeleton of the paired fins of Elasmobranchii, considered in relation to its bearings on the nature of the limbs of the vertebrata., Proc Zool Soc Lond (1881) 656-671
[9] R. Freitas, G. Zhang, M.J. Cohn, Evidence that mechanisms of fin development evolved in the midline of early vertebrates, Nature, 442 (2006) 1033-1037.
[10] P. Janvier, The paired fins of anaspids: one more hypothesis about their function, Journal of Paleontology, 61 (2015) 850-853.
[11] C. Gegenbaur, Elements of Comparative Anatomy, MacMillan, London, 1878.
[12] R. Cloutier, A.M. Clement, M.S.Y. Lee, R. Noel, I. Bechard, V. Roy, J.A. Long, Elpistostege and the origin of the vertebrate hand, Nature, 579 (2020) 549-554.
[13] E.B. Daeschler, N.H. Shubin, F.A. Jenkins, Jr., A Devonian tetrapod-like fish and the evolution of the tetrapod body plan, Nature, 440 (2006) 757-763.
[14] C. Darwin, On the origin of species by means of natural selection, or, The preservation of favoured races in the struggle for life., London : J. Murray1859.
[15] T.A. Stewart, J.B. Lemberg, N.K. Taft, I. Yoo, E.B. Daeschler, N.H. Shubin, Fin ray patterns at the fin-to-limb transition, Proc Natl Acad Sci U S A, 117 (2020) 1612-1620.
[16] M.I. Coates, The Origin of Vertebrate Limbs, Development, (1994) 169-180.
[17] M.B. Hawkins, K. Henke, M.P. Harris, Latent developmental potential to form limb-like skeletal structures in zebrafish, Cell, 184 (2021) 899-911 e813.
[18] T. V, J. Nickel, T. D, Missense Mutations in GDF-5 Signaling: Molecular Mechanisms Behind Skeletal Malformation, Mutations in Human Genetic Disease2012.
[19] M. Zhu, X. Yu, Stem sarcopterygians have primitive polybasal fin articulation, Biology Letters, 5 (2009) 372-375.
[20] N.H. Shubin, E.B. Daeschler, F.A. Jenkins, The pectoral fin of Tiktaalik roseae and the origin of the tetrapod limb, Nature, 440 (2006) 764-771.
[21] C. Minguillon, J.J. Gibson-Brown, M.P. Logan, Tbx4/5 gene duplication and the origin of vertebrate paired appendages, 106 (2009) 21726-21730.
[22] M. Logan, Finger or toe: the molecular basis of limb identity, Development, 130 (2003) 6401-6410.
[23] J. Gros, C.J. Tabin, Vertebrate Limb Bud Formation Is Initiated by Localized Epithelial-to-Mesenchymal Transition, Science, 343 (2014) 1253-1256.

[24] Q. Mao, H.K. Stinnett, R.K. Ho, Asymmetric cell convergence-driven zebrafish fin bud initiation and pre-pattern requires Tbx5a control of a mesenchymal Fgf signal, Development, 142 (2015) 4329-4339.
[25] I. Delgado, G. Giovinazzo, S. Temino, Y. Gauthier, A. Balsalobre, J. Drouin, M. Torres, Control of mouse limb initiation and antero-posterior patterning by Meis transcription factors, Nat Commun, 12 (2021) 3086.
[26] L. Jin, J. Wu, S. Bellusci, J.-S. Zhang, Fibroblast Growth Factor 10 and Vertebrate Limb Development, Frontiers in Genetics, 9 (2019).
[27] G.H. Lin, L. Zhang, Apical ectodermal ridge regulates three principal axes of the developing limb, J Zhejiang Univ Sci B, 21 (2020) 757-766.
[28] S.F. Gilbert, Developmental Biology, 6 ed., Sinauer Associates, Inc2000.
[29] H. Grandel, S. Schulte-Merker, The development of the paired fins in the Zebrafish (Danio rerio), Mechanisms of Development, 79 (1998) 99-120.
[30] K.L. Cooper, J.K. Hu, D. ten Berge, M. Fernandez-Teran, M.A. Ros, C.J. Tabin, Initiation of proximal-distal patterning in the vertebrate limb by signals and growth, Science, 332 (2011) 1083-1086.
[31] P. Thorogood, The Development of the Teleost Fin and Implications for Our Understanding of Tetrapod Limb Evolution, in: J.R. Hinchliffe, J.M. Hurle, D. Summerbell (Eds.) Developmental Patterning of the Vertebrate Limb, Springer US, Boston, MA, 1991, pp. 347-354.
[32] A. Paco, R. Freitas, Hox D genes and the fin-to-limb transition: Insights from fish studies, Genesis, 56 (2018).
[33] J. Zhang, P. Wagh, D. Guay, L. Sanchez-Pulido, B.K. Padhi, V. Korzh, M.A. Andrade-Navarro, M.A. Akimenko, Loss of fish actinotrichia proteins and the fin-to-limb transition, Nature, 466 (2010) 234-237.
[34] W. Masselink, N.J. Cole, F. Fenyes, S. Berger, C. Sonntag, A. Wood, P.D. Nguyen, N. Cohen, F. Knopf, G. Weidinger, T.E. Hall, P.D. Currie, A somitic contribution to the apical ectodermal ridge is essential for fin formation, Nature, 535 (2016) 542-546.
[35] J.M. Woltering, I. Irisarri, R. Ericsson, J.M.P. Joss, P. Sordino, A. Meyer, Sarcopterygian fin ontogeny elucidates the origin of hands with digits, 6 (2020) eabc3510.
[36] R. Freitas, C. Gomez-Marin, J.M. Wilson, F. Casares, J.L. Gomez-Skarmeta, Hoxd13 contribution to the evolution of vertebrate appendages, Dev Cell, 23 (2012) 1219-1229.
[37] R. Freitas, G. Zhang, M.J. Cohn, Biphasic Hoxd gene expression in shark paired fins reveals an ancient origin of the distal limb domain, PLoS One, 2 (2007) e754.
[38] J.C. Pearson, D. Lemons, W. McGinnis, Modulating Hox gene functions during animal body patterning, Nat Rev Genet, 6 (2005) 893-904.
[39] M. Mallo, Reassessing the Role of Hox Genes during Vertebrate Development and Evolution, Trends Genet, 34 (2018) 209-217.
[40] B.J. Swalla, Building divergent body plans with similar genetic pathways, Heredity (Edinb), 97 (2006) 235-243.
[41] C. Moreau, P. Caldarelli, D. Rocancourt, J. Roussel, N. Denans, O. Pourquie, J. Gros, Timed Collinear Activation of Hox Genes during Gastrulation Controls the Avian Forelimb Position, Curr Biol, 29 (2019) 35-50 e34.
[42] J. Zakany, D. Duboule, The role of Hox genes during vertebrate limb development, Curr Opin Genet Dev, 17 (2007) 359-366.
[43] B. Xu, S.M. Hrycaj, D.C. McIntyre, N.C. Baker, J.K. Takeuchi, L. Jeannotte, Z.B. Gaber, B.G. Novitch, D.M. Wellik, Hox5 interacts with Plzf to restrict Shh expression in the developing forelimb, Proc Natl Acad Sci U S A, 110 (2013) 19438-19443.
[44] T. Yano, K. Tamura, The making of differences between fins and limbs, J Anat, 222 (2013) 100-113.
[45] R. Freitas, J.L. Gomez-Skarmeta, P.N. Rodrigues, New frontiers in the evolution of fin development, J Exp Zool B Mol Dev Evol, 322 (2014) 540-552.

[46] D. Ahn, R.K. Ho, Tri-phasic expression of posterior Hox genes during development of pectoral fins in zebrafish: implications for the evolution of vertebrate paired appendages, Dev Biol, 322 (2008) 220-233.
[47] Z. Johanson, J. Joss, C.A. Boisvert, R. Ericsson, M. Sutija, P.E. Ahlberg, Fish fingers: digit homologues in sarcopterygian fish fins, J Exp Zool B Mol Dev Evol, 308 (2007) 757-768.
[48] M.C. Davis, R.D. Dahn, N.H. Shubin, An autopodial-like pattern of Hox expression in the fins of a basal actinopterygian fish, Nature, 447 (2007) 473-476.
[49] T. Montavon, N. Soshnikova, B. Mascrez, E. Joye, L. Thevenet, E. Splinter, W. de Laat, F. Spitz, D. Duboule, A regulatory archipelago controls Hox genes transcription in digits, Cell, 147 (2011) 1132-1145.
[50] G. Andrey, T. Montavon, B. Mascrez, F. Gonzalez, D. Noordermeer, M. Leleu, D. Trono, F. Spitz, D. Duboule, A switch between topological domains underlies HoxD genes collinearity in mouse limbs, Science, 340 (2013) 1234167.
[51] J.M. Woltering, D. Duboule, The origin of digits: expression patterns versus regulatory mechanisms, Dev Cell, 18 (2010) 526-532.
[52] J.M. Woltering, D. Noordermeer, M. Leleu, D. Duboule, Conservation and divergence of regulatory strategies at Hox Loci and the origin of tetrapod digits, PLoS Biol, 12 (2014) e1001773.
[53] A.R. Gehrke, I. Schneider, E. de la Calle-Mustienes, J.J. Tena, C. Gomez-Marin, M. Chandran, T. Nakamura, I. Braasch, J.H. Postlethwait, J.L. Gomez-Skarmeta, N.H. Shubin, Deep conservation of wrist and digit enhancers in fish, Proc Natl Acad Sci U S A, 112 (2015) 803-808.
[54] R. Sheth, L. Marcon, M.F. Bastida, M. Junco, L. Quintana, R. Dahn, M. Kmita, J. Sharpe, M.A. Ros, Hox genes regulate digit patterning by controlling the wavelength of a Turing-type mechanism, Science, 338 (2012) 1476-1480.
[55] V. Salsi, M.A. Vigano, F. Cocchiarella, R. Mantovani, V. Zappavigna, Hoxd13 binds in vivo and regulates the expression of genes acting in key pathways for early limb and skeletal patterning, Dev Biol, 317 (2008) 497-507.
[56] E. Pignatti, R. Zeller, A. Zuniga, To BMP or not to BMP during vertebrate limb bud development, Semin Cell Dev Biol, 32 (2014) 119-127.
[57] R.N. Wang, J. Green, Z. Wang, Y. Deng, M. Qiao, M. Peabody, Q. Zhang, J. Ye, Z. Yan, S. Denduluri, O. Idowu, M. Li, C. Shen, A. Hu, R.C. Haydon, R. Kang, J. Mok, M.J. Lee, H.L. Luu, L.L. Shi, Bone Morphogenetic Protein (BMP) signaling in development and human diseases, Genes Dis, 1 (2014) 87-105.
[58] D. Ben-Zvi, B.Z. Shilo, A. Fainsod, N. Barkai, Scaling of the BMP activation gradient in Xenopus embryos, Nature, 453 (2008) 1205-1211.
[59] J.W. Lowery, V. Rosen, The BMP Pathway and Its Inhibitors in the Skeleton, Physiol Rev, 98 (2018) 2431-2452.
[60] D.P. Brazil, R.H. Church, S. Surae, C. Godson, F. Martin, BMP signalling: agony and antagony in the family, Trends in Cell Biology, 25 (2015) 249-264.
[61] J.T. Thomas, D. Eric Dollins, K.R. Andrykovich, T. Chu, B.G. Stultz, D.A. Hursh, M. Moos, SMOC can act as both an antagonist and an expander of BMP signaling, Elife, 6 (2017).
[62] J. Castro, V. Beviano, A. Paco, J. Leitao-Castro, F. Cadete, M. Francisco, R. Freitas, Hoxd13/Bmp2-mediated mechanism involved in zebrafish finfold design, Sci Rep, 11 (2021) 7165.
[63] D.M. Maatouk, K.S. Choi, C.M. Bouldin, B.D. Harfe, In the limb AER Bmp2 and Bmp4 are required for dorsal-ventral patterning and interdigital cell death but not limb outgrowth, Dev Biol, 327 (2009) 516-523. [64] C.B. Kimmel, W.W. Ballard, S.R. Kimmel, B. Ullmann, T.F. Schilling, Stages of Embryonic Development of the Zebrafish, DEVELOPMENTAL DYNAMICS, (1995) 255-310.
[65] K. Im, S. Mareninov, M.F.P. Diaz, W.H. Yong, An Introduction to Performing Immunofluorescence Staining, Methods Mol Biol, 1897 (2019) 299-311.
[66] J.W. Lichtman, J.A. Conchello, Fluorescence microscopy, Nat Methods, 2 (2005) 910-919.
[67] R. Mateus, L. Holtzer, C. Seum, Z. Hadjivasiliou, M. Dubois, F. Julicher, M. Gonzalez-Gaitan, BMP Signaling Gradient Scaling in the Zebrafish Pectoral Fin, Cell Rep, 30 (2020) 4292-4302 e4297.

[68] D. Inoue, J. Wittbrodt, One for all--a highly efficient and versatile method for fluorescent immunostaining in fish embryos, PLoS One, 6 (2011) e19713.
[69] S. Gregersen, Fluorescent Peptide-Stabilized Silver-Nanoclusters, Department of Chemistry, Uiversity of Copenhagen, Kemisk Institut, 2014, pp. 171.
[70] M. Kubista, J.M. Andrade, M. Bengtsson, A. Forootan, J. Jonak, K. Lind, R. Sindelka, R. Sjoback, B. Sjogreen, L. Strombom, A. Stahlberg, N. Zoric, The real-time polymerase chain reaction, Mol Aspects Med, 27 (2006) 95-125.
[71] R. Casadei, M.C. Pelleri, L. Vitale, F. Facchin, L. Lenzi, S. Canaider, P. Strippoli, F. Frabetti, Identification of housekeeping genes suitable for gene expression analysis in the zebrafish, Gene Expr Patterns, 11 (2011) 271-276.
[72] C.J. Neumann, H. Grandel, W. Gaffield, S. Schulte-Merker, C. Nüsslein-Volhard, Transient establishment of anteroposterior polarity in the zebrafish pectoral fin bud in the absence of sonic hedgehog activity, Development 126 (1999) 4817-4826.
[73] C. Vannahme, N. Smyth, N. Miosge, S. Gosling, C. Frie, M. Paulsson, P. Maurer, U. Hartmann, Characterization of SMOC-1, a novel modular calcium-binding protein in basement membranes, J Biol Chem, 277 (2002) 37977-37986.
[74] C. Vannahme, S. Gosling , M. Paulsson, P. Maurer, U. Hartmann, Characterization of SMOC-2, a modular extracellular calcium-binding protein, J Biol Chem, 373 (2003) 805-814.
[75] D.A. Stafford, L.J. Brunet, M.K. Khokha, A.N. Economides, R.M. Harland, Cooperative activity of noggin and gremlin 1 in axial skeleton development, Development, 138 (2011) 1005-1014.
[76] Y. Furuta, B.L.M. Hogan, BMP4 is essential for lens induction in the mouse embryo, GENES & DEVELOPMENT 12 (1998) 3764–3775.
[77] S.M. Brugger, A.E. Merrill, J. Torres-Vazquez, N. Wu, M.C. Ting, J.Y. Cho, S.L. Dobias, S.E. Yi, K. Lyons, J.R. Bell, K. Arora, R. Warrior, R. Maxson, A phylogenetically conserved cis-regulatory module in the Msx2 promoter is sufficient for BMP-dependent transcription in murine and Drosophila embryos, Development, 131 (2004) 5153-5165.
[78] C. Thisse, B. Thisse, High Throughput Expression Analysis of ZF-Models Consortium Clones., ZFIN, 2005.
[79] J. Cervera, S. Meseguer, S. Mafe, The interplay between genetic and bioelectrical signaling permits a spatial regionalisation of membrane potentials in model multicellular ensembles, Sci Rep, 6 (2016) 35201.
[80] H.B. Wood, S.J. Ward, G.M. Morriss-Kay, Effects of All-trans-RetinoicAcid on Skeletal Pattern, 5'HoxD Gene Expression, and RARP2/P4 Promoter Activity in Embryonic Mouse Limbs DEVELOPMENTAL GENETICS, (1996) 74-84.
[81] J. Ka, J.D. Kim, B. Pak, O. Han, W. Choi, H. Kim, S.W. Jin, Bone Morphogenetic Protein Signaling Restricts Proximodistal Extension of the Ventral Fin Fold, Front Cell Dev Biol, 8 (2020) 603306.
[82] K.S. Choi, C. Lee, D.M. Maatouk, B.D. Harfe, Bmp2, Bmp4 and Bmp7 are co-required in the mouse AER for normal digit patterning but not limb outgrowth, PLoS One, 7 (2012) e37826. [
83] T.M. Williams, M.E. Williams, J.H. Heaton, T.D. Gelehrter, J.W. Innis, Group 13 HOX proteins interact with the MH2 domain of R-Smads and modulate Smad transcriptional activation functions independent of HOX DNA-binding capability, Nucleic Acids Res, 33 (2005) 4475-4484.
[84] Y. Lallemand, M.A. Nicola, C. Ramos, A. Bach, C.S. Cloment, B. Robert, Analysis of Msx1; Msx2 double mutants reveals multiple roles for Msx genes in limb development, Development, 132 (2005) 3003-3014.